NOVA SCHOOL OF SCIENCE & TECHNOLOGY

DEPARTAMENT OF MATERIALS SCIENCE

CAROLINA NEVES LOURENÇO

BSc in Micro and Nanotechnology Engineering

Development of a skin-like sensor for monitoring an inflammatory biomarker for wound care application

MASTER IN MICRO AND NANOTECHNOLOGY ENGINEERING

NOVA University Lisbon

September, 2022

DEPARTAMENT OF
MATERIAL SCIENCE

Development of a skin-like sensor for monitoring an inflammatory biomarker for wound care application

CAROLINA NEVES LOURENÇO

BSc in Micro and Nanotechnology Engineering

Adviser: Dr. Gabriela Martins
Researcher, BioMark/ ISEP

Co-advisers: Dr. Rui Igreja
Assistant Professor, NOVA University Lisbon

Dr. Felismina Moreira
Researcher, BioMark/ ISEP

Examination Committee:

Chair: Dr. Hugo Manuel Brito Águas,
Associate Professor, FCT-NOVA

Rapporteurs: Dr. José Ricardo Ramos Franco Tavares,
Associate Professor, FCT-NOVA

Adviser: Dr. Gabriela Ferreira de Vasconcelos Martins,
Researcher, BioMark/ ISEP

MASTER IN MICRO AND NANOTECHNOLOGY ENGINEERING

NOVA University Lisbon
September, 2022

Development of a skin-like sensor for monitoring an inflammatory biomarker for wound care application

ACKNOWLEDGMENTS

It is with a great feeling of satisfaction and accomplishment that I deliver this work. The completion of this dissertation marks the end of an important stage in my life and as such, I would like to thank all those who accompanied me.

First, I want to thank my institution, the great NOVA School of Sciences and Technologies and the Department of Materials Science for allowing me to have the best university experience I could have imagined over these five years and to the institution that took me and made this work possible – Biomark.

To my advisor Dr. Gabriela Martins, who guided and challenged me throughout this process, a huge thank you for all the support, for never having stopped believing in my work and my success and for always having a friendly word to say. I would also like to thank my co-supervisor Dr. Rui Igreja, for allowing me to establish a link between Biomark and CENIMAT and for his help and guidance throughout the entire process.

To Dr. Felismina Moreira, for welcoming me at Biomark and for always following my work and ensuring that I had the best experience. To the entire Biomark team for having received me so well, highlighting Joana Guerreiro, Daniela Oliveira, Yuselis Guerrero, Sofia Calvet and Raquel Pereira for all the time spent together, for all their kindness and for making the time away from home more bearable.

To João Santos, who helped me a lot in the transition to this new challenge and for showing me that it is not that scary after all. To Cátia Figueiredo, Mariana Cortinhal, Inês Santos, Ana Santa and Joana Pinto, a big thank you for all the guidance during my work at CEMOP and for never leaving one of my thousands of emails unanswered.

To Bia Valente, for joining me in all my adventures, for never ceasing to believe in me and for giving me the best home away from my birth home and may there always be - SUCCESS. To Carolina Viegas and Bárbara Dias, for making these college years funnier and more enjoyable. To Sara Oliveira for accompanying me since the mornings in high school, and who, together with Vicente Gonçalves and Zé Ferreira, gave me the best dinners, the best get-togethers and the best conversations into the night.

To Catarina Carmo, my Carminho, for being the best friend I could have asked to accompany me in these five years, for being there for me through the good times and the bad times and for never turning down lunch at some random new place. To Palaio, who never stopped believing that I was capable of anything, including following Tony Stark's legacy, for all the coffees and late-night talks.

To my sister, for giving me the privilege of becoming a big sister, for growing up with me and for bringing more colour to my life, and of course, for also bringing our lovely kittens into our home. To my parents who always did everything they could to ensure that I would have a role in science, even when I told them I wanted to take a course where "you can't see anything", or when I told them I was going to another end of the country to do my thesis, but never failing to ensure that I followed my path with a healthy mind. Someone once said, " they say to never meet your heroes, but if you're lucky enough you get them as your parents". To the rest of my family, for all the support and love.

To João Daniel, my love, for all the bus trips to Porto when I felt alone, for always being my support and for always motivating me and never ceasing to believe in my success.

“I have in me all the dreams in the world.” (Fernando Pessoa).

ABSTRACT

Globally, wound management poses a massive challenge with a great impact on social-economic and healthcare systems. In a post-Covid era, at-home diagnostic and monitoring devices gained a crucial role in our lives, boosting the development of novel skin patch sensors targeted for health monitoring. In this context, one of the most important requirements concerns the creation of flexible and conformable conductive platforms that can be employed as skin-like sensors. Thus, the main goal of this dissertation consists in the development of a flexible electrochemical biosensing device for the detection of an inflammation biomarker, interleukin-6 (IL-6). The 3-electrode gold pattern was standardized by e-beam evaporation on a 6 μm polyimide membrane, a transparent and biocompatible polymeric material. Subsequently, protein-printed sensors were electrochemically fabricated on the gold-modified electrodes for IL-6 detection. This biorecognition is accomplished with molecularly-imprinted polymers (MIPs) that were synthesized on the electrode surface by electropolymerization of a mixture of two monomers, pyrrole and carboxylated pyrrole. Along this process, several electropolymerization parameters were optimized like the potential range and number of cycles, as well as the pH conditions of the medium and the removal of the imprinted protein, to create the cavities responsible for the rebinding event. Electrochemical sensing features were then investigated to demonstrate the imprinting effect and the optimized biosensor exhibited a linear electrochemical response in the 0.5 ng/mL to 500 ng/mL concentration range. Moreover, chemical, and morphological characterizations, such as XPS, SEM and FTIR confirmed the surface modifications on the gold surface. The final biosensing device demonstrated great potential in terms of sensitivity, stability, and reproducibility, making it a simpler and more cost-effective portable solution for the remote monitoring of chronic wounds. Finally, the incorporation of the sensing component directly on biocompatible flexible polymers enables new monitoring and treatment tools that can be more accurate, less invasive, and more comfortable for the patient.

Keywords: biosensor; molecularly-imprinted polymer; flexible substrate; gold-based electrodes; electrochemical; interleukin; polyimide

RESUMO

Globalmente, a monitorização de feridas representa um enorme desafio com grande impacto nos sistemas socio-económicos e de saúde. Numa era pós-Covid, os dispositivos de diagnóstico e monitorização a partir de casa adquiriram um papel crucial nas nossas vidas, impulsionando o desenvolvimento de novos sensores flexíveis para a pele para monitorização da saúde. Nesse contexto, um dos requisitos mais importantes diz respeito à criação de plataformas condutoras flexíveis e conformáveis que possam ser utilizadas como sensores para pele. Assim, o principal objetivo desta dissertação consiste no desenvolvimento de um dispositivo biossensor eletroquímico flexível para a deteção de um biomarcador de inflamação, interleucina-6 (IL-6). O padrão de 3 elétrodos de ouro foi padronizado por evaporação por feixe eletrónico numa membrana de poliimida com 6 µm de espessura, um material polimérico transparente e biocompatível. Posteriormente, os biossensores foram fabricados eletroquimicamente nos elétrodos modificados com ouro para deteção de IL-6. Este bioreconhecimento é realizado através de polímeros de impressão molecular (MIPs) que foram sintetizados na superfície do elétrodo por eletropolimerização de uma mistura de dois monómeros, pirrol e pirrol carboxilado. Ao longo deste processo, vários parâmetros de eletropolimerização foram otimizados tais como a gama de potencial aplicado e o número de ciclos, as condições de pH do meio e a remoção da proteína impressa, a fim de criar as cavidades responsáveis pelo evento de religação. As características de deteção eletroquímica foram então investigadas para demonstrar o efeito de impressão e o biossensor otimizado exibiu uma resposta eletroquímica linear na gama de concentrações de 0.5 ng/mL a 500 ng/mL. Além disso, caracterizações químicas e morfológicas, tais como XPS, SEM e FTIR confirmaram as modificações químicas na superfície do eléctrodo. O dispositivo biossensor final demonstrou potencial em termos de sensibilidade, estabilidade e reprodutibilidade, tornando-se uma solução portátil, simples e económica para a monitorização remota de feridas crónicas. Por fim, a incorporação do componente sensor diretamente em polímeros flexíveis biocompatíveis permite novas ferramentas de monitorização e tratamento que podem ser mais precisas, menos invasivas e mais confortáveis para o paciente.

Palavras chave: biossensor; polímero de impressão molecular; substrato flexível; elétrodos de ouro; eletroquímico; interleucina; poliiamida

CONTENTS

LIST OF FIGURES

ACRONYMS

ATR	Attenuated total reflection
CE	Counter electrode
CV	Cyclic voltammetry
DFU	Diabetic foot ulcers
DI	Deionization water
DPV	Differential pulse voltammetry
EDOT	3,4-ethylenedioxythiophene
EIS	Electrochemical impedance spectroscopy
FTIR	Fourier transform infrared spectroscopy
IL-6	Interleukin 6
IPA	Isopropyl alcohol
MIP	Molecularly-imprinted polymer
NIP	Non-imprinted polymers
OCP	Open circuit potential
o-PDA	O-phenylenediamine
POC	Point-of-care
PVA	Poly (vinyl alcohol)
Py	Pyrrole
RE	Reference electrode
Sa	Electroactive area
SEM	Scanning electron microscope
Sg	Geometric area
SPE	Screen-printed electrode
TNF	Tumor necrosis factor
WE	Working electrode
XPS	X-ray photoelectron spectroscopy
XRD	X-ray diffraction

SYMBOLS

A	Electrode area
[C]	Mass concentration of the analyte
Cdl	Double layer capacitance
D	Diffusion coefficient of the analyte
Ip	Peak current intensity
n	Number of electrons transferred in the electrochemical reaction
Rct	Charge-transfer resistance
Rs	Solution resistance
v	Scan-rate
Zw	Warburg resistance

1 INTRODUCTION

1.1 Wound care

Wounds that do not heal, also known as chronic wounds, are important health issues that affect a large number of individuals, imposing a significant financial burden to the health care. This load is growing as healthcare costs rise, the population ages, and the prevalence of comorbidities such as diabetes rises [1]. In this context, diabetic foot ulcers (DFU) are one of the most common and costly complications of diabetes, affecting more than 10% of all diabetic individuals along their lifetime, that ultimately, can result in limb amputations.

Wound healing is composed by a complex series of biological responses that have traditionally been managed using conventional dressing and bandage materials [2],[3]. However, the concept of diagnostic sensors fully integrated to enable wound monitoring and treatment is growing rapidly, and there is a lot of interest for applying this innovative technology in the chronic wound context [4].

The most prevalent approach to wound assessment today is through a basic visual inspection, which results in a subjective and sometimes unpleasant outcome. For this inspection, the dressing must be removed and replaced, which contributes to the patient's discomfort. Furthermore, due to the lack of suitable monitoring approaches using relevant biomarkers for a continuous assessment, health personnel are unaware of the efficiency of wound management when the patient is at home. The ability to track the progress of the wound condition even when the patient is not hospitalized would allow for more specific and faster treatment, if needed, since the increased number of visits due to the need to continuously monitor the healing process raises the cost of treatment and increases stress in medical centres [1], [4].

1.2 Inflammation

The wound healing process in chronic wounds is heavily controlled by distinct cellular players of the skin that normally progresses through distinct inflammatory, proliferative, and maturation phases [5]. Inflammation is an essential innate immune response provided by the immune system to ensure survival against infections and injuries. Inflammatory responses are critical for maintaining normal tissue homeostasis, that is, a stable condition for the organism to perform its physiological functions properly [6]. The primary players in the inflammatory phase include the release and resolution of a variety of cytokines (such as IL-1β, IL-6, and IL-8), blood components, neutrophils and macrophages, and changes in oxygen concentration and pH in the wound [7].

Thus, collecting information related to the presence of biomarkers like cytokines, that are closely connected with the progression of the wound, can give a valuable input in terms of diagnostic and therapeutic applications. Briefly, cytokines are small, secreted proteins that are practically produced by all cells to regulate and impact the immune response [8]. They can be categorized based on their functions, or on their structure [9]. Herein, special emphasis was given to IL-6 that is a pro-inflammatory cytokine (function) and belongs to the interleukin family (structure). IL-6 is involved in chronic inflammation (which is strongly linked to chronic inflammatory diseases, autoimmune diseases, and cancer) as well as the cytokine storm of coronavirus disease 2019 (COVID-19), a type of inflammation in which the production of inflammatory cytokines is acutely induced in a dysregulated way in response to some stimuli [10].

Although IL-6 has unquestionable predictive significance in early inflammation, no considerable advances in therapeutic applications have been made, and many doctors continue to use a combination of clinical presentation, white blood cells count, C-reactive protein levels, and fever measurement over pricey IL-6 determination [8]. With the challenges of cytokine detection, such as intricate cytokine signalling, dynamic secretion, low concentration, and low stability, the development of novel detection platforms and materials for producing point-of-care (POC) cytokine biosensors has grown in the last years [9]. Despite various studies can be found in literature regarding different approaches to detect and quantify IL-6 presence, most of them are time-consuming, expensive, and complex methodologies, making it not compatible for routine use [11], [12].

1.3 Biosensor

Over the last decades, alongside with digital evolution, biosensor development has suffered a great transformation and application in distinct fields like food safety, environment, healthcare, sportswear, pharmacology, etc.[13], [14] . A biosensor is a device or probe that produces a measurable signal based on the concentration of a biological substance, known as an analyte [15]. A typical biosensor consists of the following components: an analyte (the substance under research to be detected), a bioreceptor (the element that is responsible for recognizing the analyte), a transducer (the element that converts the biorecognition event into a measurable signal directly related to the amount of analyte present), electronics (the signal is amplified, converted to digital format, and quantified by the display element), and display (the user interpretation system that can be presented in numerical value, graph or figure) [16].

Certain important requirements must be met to develop a highly effective biosensor system with potential to be commercially used. These requirements include: selectivity (the bioreceptor must be able to detect a specific target analyte molecule in a sample containing unwanted contaminants), limit of detection (the minimum amount of analyte that can be detected/identified correctly and at low concentrations), linearity (the higher the linearity, the greater the detection of the substrate concentration), the response time (the time required to obtain 95% of the data, which should be kept to a minimum), reproducibility (defined by precision and accuracy, the biosensor must generate equal findings each time the sample is measured), stability (is the vulnerability to environmental disturbances inside and outside the biosensor device, is one of the key characteristics as continuous monitoring is required) [16].

1.3.1 Recognition element

The analytical specificity is conferred by the biorecognition system that is a crucial phenomenon for successful biosensing outcomes. Biosensors can be classified according to their type of biorecognition element, being the most common one, antibodies, nucleic acids, enzymes, and cells [17]. Although most of these recognition elements present high selectivity and sensitivity response, their main limitations concern stability over-time and cost issues. Therefore, molecularly-imprinted polymers (MIPs) appeared as an alternative to design synthetic materials, holding higher stability and robustness, with the ability to mimic the behaviour of natural biomolecules.

MIPs are polymeric matrices that can recognize and attach to specific molecules in a selective manner. The molecular imprinting approach involves the polymerization of monomers in the presence of a target analyte, which serves as a template during polymer synthesis. The affinity of the resultant products is expected to be comparable to that of the antibody-antigen affinity. Thus, the analyte is recognized in the cavities created in the polymer matrix. Three main processes are involved in the formation of these cavities: interaction between the template and functional monomers that form a complex during imprinting and rebinding; polymerization of the resultant complex; and, finally, removal of the imprinted template [18].

The nature of the functional monomers, crosslinking agents and initiators, solvents, reagent ratio, polymerization technique, and imprinting approach are all elements to consider [19]. The end product is a stable polymer capable of rebinding the target molecule and with modulable properties such as stiffness, porosity, molecular weight, resistance, and responsiveness to diverse stimuli, hence the interest in its application in biosensors. Furthermore, the introduction of MIP-based materials as biorecognition element has been widely explored mostly due to its facile operation, simple equipment and mild conditions.

The imprinting of the complementary cavities can be performed through two different approaches that includes, bulk and surface, with the latter being employed in this dissertation. In the bulk imprinting method, the surface of the transducer is coated with a prepolymer mixture that also includes the template molecule. These interact with one another to form a network, which is then polymerized in a one-step procedure. Finally, the template is removed, leaving cavities throughout the material with shape and size specific for recognizing the analyte under study. This approach is most suited and commonly employed for creating cavities for small molecules. However, the main limitation results in a smaller number of useful printed places in the polymer matrix for rebinding. To overcome this drawback and others like delayed kinetics, incomplete template removal, and low mass transfer, various strategies for locating binding sites primarily on the surface are presented, being surface imprinting one of them [19],[20]. As the target molecule is previously deposited on the surface of the substrate, the imprinted binding sites are generated and positioned near to the surface of the polymer, allowing the creation of thin polymeric films. As a result, the printed set is more resilient and simpler to integrate into electrochemical platforms, while also providing access to bigger target analytes. This method improves the surface-to-volume ratio and the available locations for rebinding, thus increasing sensitivity and selectivity [21].

1.3.2 Signal transduction

Another way to categorize MIP-based sensors is through the nature of the transduction element. For instance, transducers can be classified into electrochemical, optical, thermal, electrical, and gravimetric types based on their functioning principles. Although the selection of the transducer is an important aspect to obtain the desirable sensitivity and selectivity, herein the focus of this work was to develop biomimetic materials using electrochemical transduction as a quick, low-cost and quite sensitive approach

So, electrochemical biosensors are designed to transform the effect of the electrochemical interaction between the analyte and the electrode surface into a measurable electrical signal. An electrochemical reaction between the bioreceptor and the analyte occurs on the surface of the transducer, creating observable electrochemical signals in the form of voltage, current, impedance, and capacitance. Thus, electrochemical biosensors can be sub-divided based on the transduction principle into: potentiometric (measures the charge accumulated on the working electrode relative to the reference electrode), amperometric (measures the current produced due to electrochemical oxidation or reduction of electroactive species in the working electrode), impedimetric (measures the electrical impedance variation at the electrode/electrolyte interface), conductometric (measures the change in conductance between the pair of electrodes due to the electrochemical reaction) and voltammetric (measures the current through the controlled variation of the applied potential) [16]. Moreover, the use of electrochemical biosensors can occur under two different ways, direct and indirect, if a redox mediator is required or not to promote reversible electrochemical processes.

Besides the wide range of applications and simple instrumentation, electrochemical sensing technology enables to achieve high level of sensitivity, selectivity, and detection capabilities.

1.3.2.1 Electropolymerization

In the context of electrochemical biosensors that employ MIPs as biorecognition systems, one of the most used techniques is electrochemical polymerization or electropolymerization.

Electropolymerization is a simple procedure in which a potential or range of potentials are applied to a solution containing electroactive monomer molecules and/or biomolecules. Briefly, at the electrode surface, the monomer is reduced or oxidized, producing reactive radical species that combine to form a polymer [16]. A controllable thickness polymer can be generated by modifying the electrochemical parameters such as the applied potential range, the number of cycles, and the sweep rate. Furthermore, this in-situ technique allows the growth of a polymeric film with different shapes and sizes directly in the conductive substrate. The selectivity of the electrosynthesized MIP can also be enhanced by altering the monomers with additional functional groups [21].

Since the electrosynthesis of MIPs involves both conducting and insulating/non-conducting polymers, the method of choice for signal transduction is linked to the conductivity of the polymer. Non-conductive polymers can be more sensitive to impedance changes; however, their electrochemical deposition must be managed since their growth becomes terminated when the polymer isolates the surface of the fundamental conductive electrode. Deposition of conductive polymers, on the other hand, can continue indefinitely since the deposition conditions regulate the thickness of the polymer [21].

The most common electrochemical technique used for applying the potential (range) that will electropolymerize the monomer mixture is cyclic voltammetry (CV). It is the most versatile technique and is frequently the initial step in an electrochemical study at the electrode surface. A typical electrochemical cell is constituted by 3 electrodes: working electrode (WE), reference electrode (RE) and auxiliary/counter electrode (CE). Between a WE and a RE, the potentiostat applies the desired potential signal (which sweeps the electrode potential between two values). The WE is the one where the redox reaction of interest occurs, the RE maintain the constant equilibrium potential and the CE is responsible for supplying the current that keeps the redox reaction going. A great advantage of using CV technique results from its ability to detect redox behaviour in a wide range of potential with high sensitivity, which results in voltamograms with current values in response to an energy variation [22].

Electrochemical impedance spectroscopy (EIS) is another powerful electrochemical technique with great relevance for the detection of relevant biological markers. This method applies a stimulus to the electrode, based on an alternating signal, a potential is applied and the resulting current is measured. The response measures the impedance of a system over a range of frequencies and, therefore, the frequency response of the electrochemical system remains in relation to the electrical resistance [23]. The electrochemical processes associated with electrolyte/interface and redox reactions are simulated as an electrical circuit that is designed and implemented to understand and evaluate the EIS system's individual components: solution resistance (*Rs*), double layer capacitance at the electrode surface (*Cdl*), charge-transfer resistance (*Rct*), and Warburg resistance (*Zw*). As a result, Nyquist plots are obtained through an EIS measurement arising as the most critical data to gather for surface properties on simulated electrical circuit fitting [24].

Nowadays, most of the electrochemical biosensors have been developed in miniaturized conductive platforms, such as, screen-printed electrodes (SPEs). This popular version allows minimal volumes of samples, portability and in some-cases, low-cost technology. For instance, Gonçalves et al. reported an electrochemical sensor with an imprinted polymeric film produced by co-electropolymerization of pyrrole (Py) and carboxylated pyrrole (Py-COOH) to detect the presence of IL-6 [25]. Ozcan et al., presented a novel MIP-based biosensor made of graphene quantum dots and functionalized with multi-walled carbon nanotubes composite for IL-6 protein detection [26]. Although these approaches enabled quick responses, good

sensitivity and reproducibility, most of these conductive platforms are mechanically rigid and not compatible to be used in skin-like devices.

1.4 Wearable biosensors

Wearable sensing devices have recently emerged as an advanced and personalized approach to real-time wound monitoring, as the incorporation of diagnostic instruments into dressings to detect physiologically relevant parameters can provide useful information for diagnostic and therapeutic purposes [5]. Recently, there has been a significant advance in the development of lightweight, flexible, and wearable physical sensors with unique characteristics, such as, high degrees of deformability and conformability on surfaces of various geometries, long-term stability, increased sensitivity, and excellent optical transparency [27].

Because of their high specificity, speed, portability, low cost, and low power consumption, biosensors hold great promise for wearable applications. They are gaining popularity due to their ability to give continuous, real-time physiological information via dynamic, non-invasive assessments of biochemical markers in biofluids [28].

Wearable biosensors can help users avoid uncomfortable and risky blood sample procedures and can be seamlessly integrated into their daily routine. To achieve this capability, the biosensor platform must allow direct contact with the sample biofluids while causing no discomfort to the user. This bodily compliance can be achieved by using modern materials and smart designs that provide the required flexibility and elasticity [28].

1.4.1 Polyimide

In this context, polyimides are a flexible substrate that has gained considerable use in the design of biological sensors. They are a type of polymer that has a stiff aromatic backbone structure and strong interchain connections, giving them exceptional mechanical, chemical, and thermal durability. Many film properties, such as Young's modulus, coefficient of thermal expansion, and dielectric constant, can be changed throughout the synthesis process, allowing polyimide with specific properties to be created. These properties are also due to the very symmetrical and highly polar groups [5].

The adherence of other materials to the polyimide film, such as gold, a substance used to create electrodes, is one of the most important qualities of a thin film primarily for this application [29]. As a result, polyimides combine good qualities for the purpose at hand, as well as flat topographies and ultra-thin films with thicknesses ranging from 1 to 5 μm [30]. As low-cost flexible materials with high biocompatibility and inert chemical behaviour, polyimides are attractive substrates for biosensors [31].

Cardoso et al. presented a biosensor platform with carbon electrodes manufactured by laser irradiation of polyimide substrates and a MIP as the biorecognition element. This biosensor detects chloramphenicol, an antibiotic present in water that is efficient against a wide range of bacteria [32]. Baraket et al. described a label-free biosensor fabricated on a gold surface that had previously been deposited in polyimide. This immunosensor was developed to detect the cytokine TNF, which is a pro-inflammatory cytokine characterized by circulating levels for chronic heart failure and patients with a left ventricular assist device, who are at high risk of mortality during the early expression of an inflammatory storm [33].

In sum, the main goal of this dissertation is the combination of a MIP material as a biorecognition system targeted for IL-6 detection with the use of polyimide-modified substrates for incorporation into wound dressings for remote continuous monitoring.

2 MATERIALS AND METHODS

2.1 Reagents

All reagents were analytical grade and used as supplied without further purification and can be found in the appendix (A.1). All experiments were performed at room temperature. Electrolyte and buffer solutions were prepared with laboratory grade Milli-Q ultrapure water.

2.2 Transducer Fabrication

2.2.1 Membrane synthesis

The first step includes proper cleaning of the glass substrates that will serve as support during membrane manufacturing. The glass substrates were cleaned in an ultrasonic bath, first 10 minutes in acetone, followed by 10 minutes in IPA. Finally, the glass was washed with ultrapure water and dried under a flow of nitrogen.

To facilitate the peel-off of the polyimide membrane, it was necessary to create a sacrificial layer between the membrane and the glass substrate. The material chosen for this purpose was PVA because it is soluble in water and easily removed. The PVA solution was prepared by mixing 5 g of PVA powder in 100 ml of deionization (DI) water (5% by weight) in a glass vial and heated to 90°C with 1000 rpm until dissolution was complete (approximately 12 hours). After cooling for 3 hours at room temperature, it was centrifuged on a previously cleaned glass substrate. The PVA was spin-coated for 10 seconds at 1000 rpm with a 500 rpm/s acceleration, followed by 20 seconds at 2000 rpm with 1000 rpm/s of acceleration. After spin-coating, the sample was heated on a hot plate during 10 min at 110°C.

Following PVA deposition, the adhesion promoter (VM652) was spin-coated for 30 seconds at 3000 rpm with a 2000 rpm/s acceleration. Polyimide 2611 was then spread on the PVA and adhesion promoter-coated substrate for 7 seconds at 500 rpm (acceleration 500 rpm/s) and 30 seconds at 3000 rpm (acceleration 500 rpm/s) to achieve a final thickness of 6 µm. The sample was then soft-baked for 90 seconds at 90°C and 90 seconds at 150°C. All spin coating deposition and consequent soft-baking were carried out in a clean room environment. The spin coating processes were conducted with a Suss Labpsin6 table-top spin coater and the metal deposition was performed with a "homemade" e-beam evaporator.

2.2.2 Gold deposition

The chosen material to make the transducer electrodes was titanium/gold 6 nm/60 nm thin film. To comply with the 3-electrode configuration, an acetate mask was laser-standardized to the size of the glass substrate. In this manner, it was possible to deposit 8 sets of 3 electrodes for each glass. A loaded gold crucible and titanium crucible, together with four glass samples with membranes and acetate masks already prepared, were placed in the chamber for 3 hours until a pressure of 3.0×10^{-6} mbar was reached. The electron beam was then directed at the crucible at a current of 0.03 mA until the titanium was melted and 6 nm of titanium was deposited. The electron beam was then directed at the gold crucible at a current of 0.03 mA to melt the gold, and a layer of 60 nm was obtained in the sample.

2.3 Electrochemical measurements

Electrochemical measurements were carried out by using a conventional 3-electrode system that consisted of a working (WE, 3 nm diameter), a counter (CE) and a pseudo-reference electrode (RE), made of the same gold material. Electrochemical measurements were performed with a Metrohm Autolab PGSTAT302N potentiostat/galvanostat equipped with a FRA2 module and controlled by Nova 1.11 software. The interface between the electrodes and the equipment was made by using a homemade interface device designed specifically for this purpose by CENIMAT.

In order to assess the electrode performance, the electroactive surface area of the electrodes was calculated by performing CV at different scan-rates (250, 150, 100, 50, 25 and 10 mV/s) using $[Fe(CN)_6]^{4-}$ redox probe in 0.1 M KCl electrolyte solution. The experiments were performed in triplicate. Then, each electrode modification was electrochemically characterized by EIS with a 5 mM solution of $K_3[Fe(CN)_6]$ and $K_4[Fe(CN)_6]$ prepared in citrate-phosphate buffer solution (0.15 M, pH 4.8), which was prepared by combining the appropriate amounts of citric acid and sodium phosphate dibasic dihydrate. All electrochemical measurements were performed by covering the three electrodes (WE, CE and RE) with a solution volume of 100 µL. The EIS experiments were carried out at open circuit potential (OCP) and over the frequency range from 0.01 Hz to 100 kHz. Between all measurements, the electrodes were washed with Millipore water and dried under nitrogen flow. The detection of IL-6 was followed by means of DPV in the potential range of -0.2 V to +0.2 V, with a scan- rate of 10 mV/s, pulse amplitude of 25 mV and a pulse width of 50 ms. All experiments were carried out at room temperature. Calibration curves were made with standard IL-6 solutions ranging from 0.05 pg/mL to 500 ng/mL.

2.4 Biosensor assembly and characterization

Initially, the modified membrane was transferred to acetate double-sided adhesive tape, as it is more stable and compatible with the interface, and a small amount of hot glue was applied below the WE in order to ensure a constant working area for all electrodes. Before use, the electrodes were electrochemically cleaned in a 0.5 mM H_2SO_4 solution with 5 voltammetric sweeps in the potential range -0.2 V to +1.2 V, with a scan- rate of 50 mV/s. Afterwards, the gold electrodes were functionalized with a thin layer of poly(o-PDA). This was performed by applying voltammetric sweeps ranging between +0.2 V and +1.0 V, at a scan- rate of 150 mV/s, in an o-PDA solution (0.5 mM). Then, 6 µl of the template molecule, IL-6 (5 ug/mL), prepared in citrate-phosphate buffer was incubated on the WE for 3 hours.

The MIP film was deposited by electropolymerization, with a solution obtained by mixing the functional monomers in the citrate-phosphate buffer solution: 2 mM of Py and 0.2 mM of Py-COOH. After optimization, the conditions used for the electropolymerization were the following: a potential range of -0.3 to +0.95 V, a scan- rate of 150 mV/s and 3 sweep cycles. To remove the template molecule, a solution of NaOH (0.1 M) was incubated on the WE for 1 hour followed by incubation in the buffer solution also for 1 hour. In parallel, control electrodes (NIPs or non-imprinted polymers) were prepared using the same procedure in the absence of the template cytokine, IL-6.

After the construction of the biosensor, it was characterized by scanning electron microscope (SEM), X-ray photoelectron spectroscopy (XPS) and Fourier-transform infrared spectroscopy (FTIR), the details of which can be found in the appendix (A.2).

3

RESULTS AND DISCUSSION

3.1 The electrode fabrication process

3.1.1 Synthesis of the membranes

One of the main steps during the membrane fabrication process concerns the PVA deposition. This procedure ensures an easy peel-off of the polyimide membrane since PVA is soluble in water [34] and so, it acts as a sacrificial layer. After optimizing the spin coating conditions, it was important to guarantee the homogeneous distribution of the PVA in order to insure complete peel off of the polyimide membrane. Afterwards, to successfully separate the polyimide membrane from the glass, the sample must come in contact with water to dissolve the PVA. Because the glass in which the polyimide was prepared has been previously cut to the size of the contacts, it was only necessary for the edges to come in contact with the humidity of the air and then, pull one of the ends to release the sample from the glass membrane.

The result turned out to be a thin, 6 µm thick, transparent membrane with a slight orange tint that comes from the polyimide (Figure 1). Thus, the final membrane fits the primary characteristics of this sort of substrate: it is flexible enough to conform to the contours of the body; it is non-toxic and does not induce immune response. Besides that, as polyimide belongs to a class of polymers with a rigid aromatic bone structure, it has high mechanical, chemical and thermal stability (up to 400 ºC)[1], [5].

Figure 1 -Final flexible polyimide membrane.

3.1.2 Deposition of gold electrodes

The intended sample configuration is the 3-electrode configuration: WE, CE and RE (Figure 2a). The same gold material was applied to all electrodes, and consequently just one single mask-step was employed. In this configuration, the WE was design to have a diameter of 3 mm and, since the 3 electrodes are all made of the same material, it was important to ensure that the CE should have a larger surface area than the WE [35].

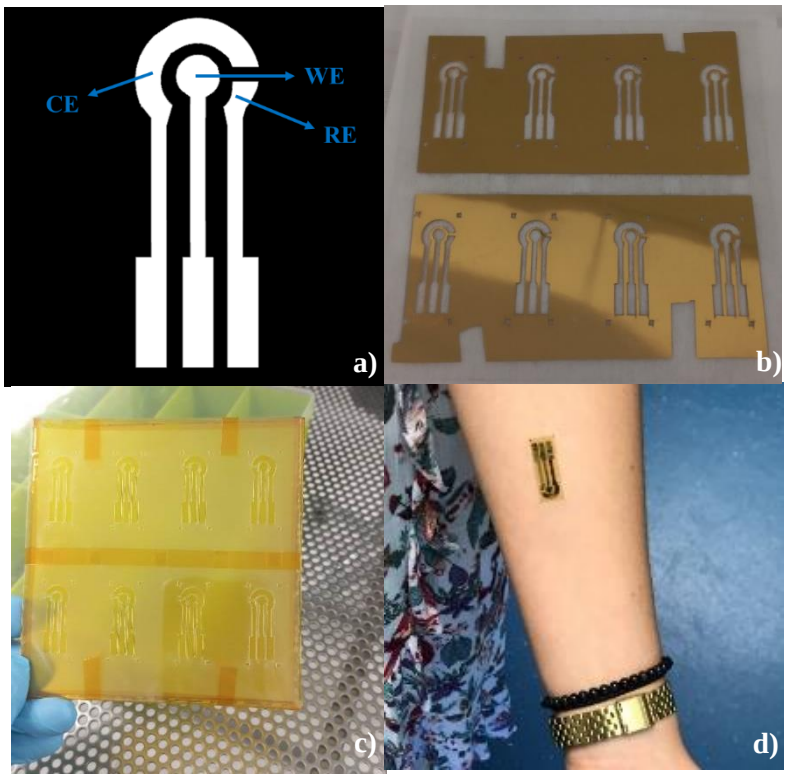

Figure 2 - a) Electrodes design; b) Acetate mask after metal deposition; c) Membrane and mask setup before loading into the e-beam; d) Final electrode device completely adhered to the skin.

Since the performance of the analytical method is highly dependent on the WE material, herein gold was chosen for this purpose because of its high conductivity, biocompatibility, and chemical stability [36]. Although this noble metal does not constitute a low-cost material, it is expected that in the future this kind of electrodes could be completely regenerate and reuse.

The gold layer was deposited by E-beam evaporation. The membrane together with a previously standardized acetate mask (Figure 2b and Figure 2c) were placed in the chamber and an electron beam (e-beam) is applied as an energy source to heat the source material and generate vaporized particles. This approach has an advantage over screen printing since it can produce ultra-thin and smooth films with excellent electrical characteristics. The deposited films are dense, compact and of low tension. Furthermore, because we are working with a very thin polyimide membrane, another benefit of this technique is that the electron beam focuses on the material that will be deposited, in this case, pure gold, rather than the sample. Also, the deposition of pure gold against the gold inks, typical of the screen-printing technique, enables the formation of films quite smooth, which represents itself a great advantage, especially in terms of electrochemical performance [37], [38].

Gold is appealing for metallization due to its high electrical conductivity and biocompatibility, however, this type of metals needs additional bonding layers for polymer adherence, since they do not easily form oxides suitable for adherence. For this purpose, a transition metal, titanium, was incorporated, which has been predominantly used to increase the interfacial bond to a dielectric substrate, in this case, the polyimide membrane, since titanium forms a passive oxide layer suitable for membrane adhesion. Because the titanium layer is very thin, being only 6 nm thick, it has no effect on the dielectric characteristics of the polyimide. In this way, the 60 nm gold layer deposited on top of the thin titanium layer completely adheres to the polyimide membrane [39]. We ended the process with a membrane completely conformable to the skin (Figure 2d), with the gold electrodes deposited and ready to be functionalized.

3.1.3 Membranes characterization

3.1.3.1 FTIR analysis

Fourier transform infrared spectroscopy (FTIR) analysis is commonly employed to identify organic, inorganic, and polymeric compounds by scanning the samples with infrared light. The information is then converted into an absorption or transmission spectrum [40].

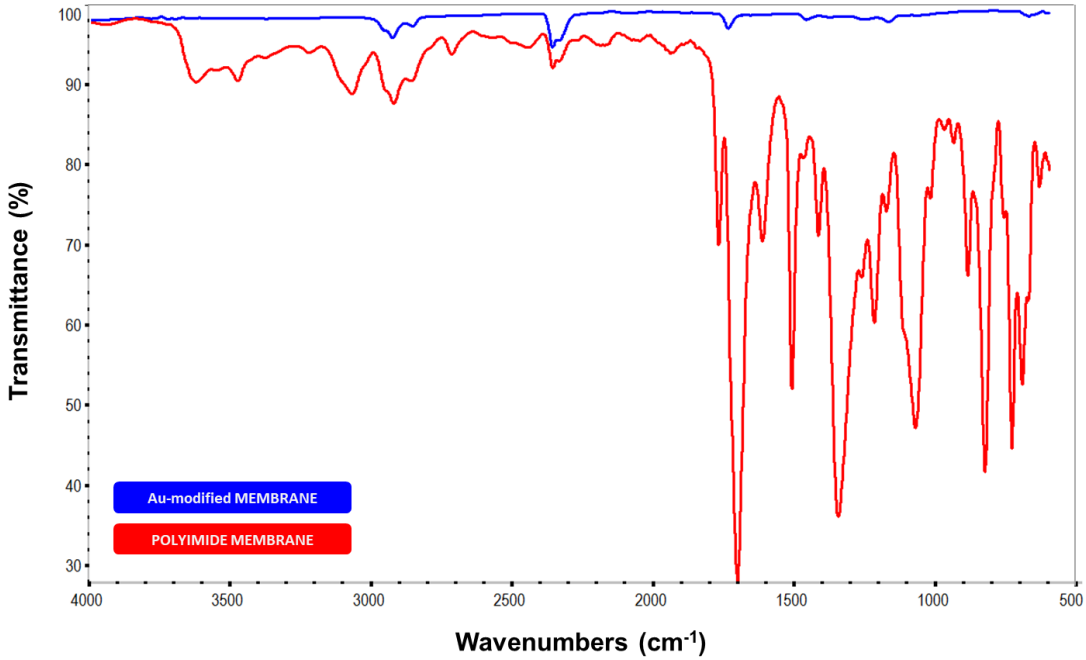

Figure 3 – ATR-FTIR analysis of the polyimide membrane before and after gold deposition.

As we can observe in Figure 3 the characteristics of the polyimide membrane are evidenced by the following absorption bands 1700 cm^{-1} (C=O asymmetric stretching), 1500 cm^{-1} (aromatic C-H); 1370 cm^{-1} (C–N symmetric stretching) and 700 cm^{-1} (C=O bending) [41]. Afterwards, the gold deposition on the membrane has been proven by the disappearance of the characteristic peaks regarding the polyimide material, that became covered by the metal material.

3.1.3.2 XRD analysis

X-ray diffraction (XRD) is used to characterize materials by measuring crystal structure, crystallite size, and deformation. It has been widely used for the analysis of thin films and materials; and it is a method that provides information about surface changes. XRD employs the Bragg equation concept, which deals with the reflection of the incidence of the collimated X-ray beam on a crystalline plane of the sample to be described [42].

The characterization data were derived from the master's thesis by J. Santos, 2022, since the protocol followed during the manufacturing of polyimides was the same. The polyimide membrane diffractogram presents a small cluster at 20º, which is typical of this material, as shown in A.3.

The diffractogram of the polyimide membrane covered with an Au layer of 80 nm revealed peaks at 2Θ=35º, 38º, 45º, and 65º, which correspond to (111), (200), (220), and (311) planes, respectively, typical of gold compounds, confirming the presence of a layer of gold on top of the polyimide sample [43].

3.2 Electrochemical characterization of the electrodes

The modified polyimide membrane was fabricated on a glass surface; however, it is necessary to understand how the electrochemical platform works in a flexible format. Since the membrane is only 6 µm thick and it can be difficult to handle with it in order to be read through the interface, it was more convenient to transfer the membrane to hard flexible substrates during the optimization tests. Herein, some approaches were tested, such as, acetate sheet with UHU glue, double-sided adhesive tape and acetate with double-sided adhesive tape, being the last one chosen for being more robust and for presenting more stable and reproducible results. To have a similar and constant defined WE for all electrodes, it was also applied a small amount of hot glue below the WE (Figure 4a). In addition, the glue also intends to protect any liquid leakage near the electric reading area on the interface (Figure 4b).

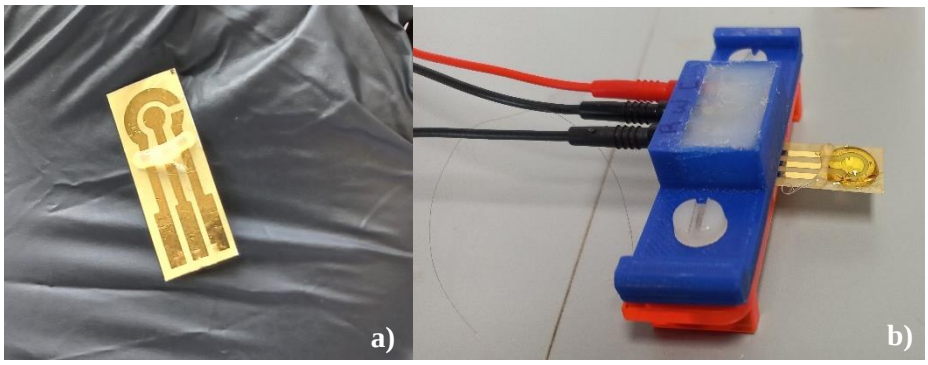

Figure 4 - (a) Final electrode configuration; (b) Electrode inserted into the interface to be analysed.

The conductive membranes were then electrochemically characterized using CV technique. In this study, voltammetric sweeps were applied at different scan-rate values using $[Fe(CN)_6]^{4-}$ as the redox probe prepared in 0.1 M KCl electrolyte solution. Each experiment was carried out in triplicate.

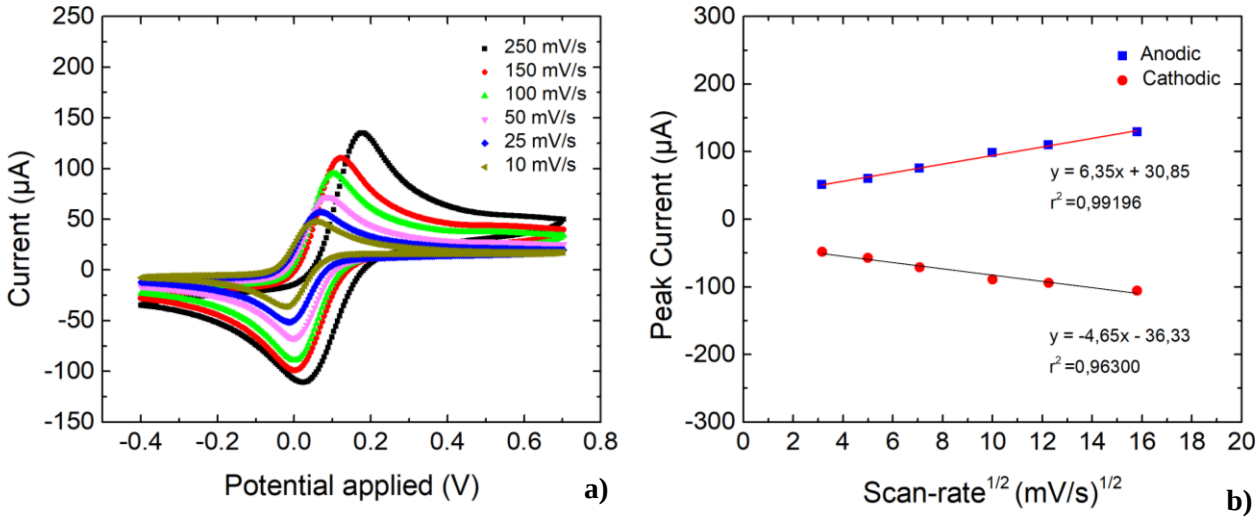

Figure 5 - (a) Cyclic voltammograms at different scan- rates; (b) Plot representation of anodic and cathodic peak currents versus the square-root of the scan-rate.

The results revealed anodic and cathodic peaks with high peak amplitudes (Figure 5a). Furthermore, when the scan-rate increases, the increasing distance between the potentials of the reduction and oxidation peaks shows the quasi-reversible redox process of $[Fe(CN)_6]^{4-}$ on the electrode surface. As a result, the anodic and cathodic peak currents were plotted against the square root of the scan-rate, revealing a dependent linear behaviour in the sweep range of 10 mV/s to 250 mV/s, which is a characteristic of a diffusion-controlled mechanism responsible for the electrochemical process that occurs on the electrode surface (Figure 5b).

As mentioned before, the nature of the electrode material and its interaction with the membrane are critical components for the electrochemical performance of the electrode. In most of these cases, the electroactive area, that is the actual area where electrons interact, differs from the geometric area of the electrode. Thus, the electroactive area of the electrode can be estimated using the Randles-Sevcik equation [44]:

$$I_p = 268600 \times n^{\frac{3}{2}} \times A \times D^{\frac{1}{2}} \times C \times \vartheta^{\frac{1}{2}}$$

Where *I*p is the peak current intensity (A), *n* is the number of electrons transferred in the electrochemical reaction, *A* is the electrode area (cm^2), *D* is the diffusion coefficient of the analyte, *C* is the mass concentration of the analyte (mol/cm^3) and *v* is the scan-rate (V/s).

Herein, it was used the slope of the graph illustrating the peak current versus the square root of the sweep rate to the previous equation to determine the electroactive area of the fabricated electrodes. The calculated electroactive electrode area was 0.527 cm^2 and the geometric area is 0.071 cm^2, and so, the *S*a/*S*g ratio, where *S*a is the electroactive area and *S*g is the geometric surface area, was 7.45. These values are not directly comparable to those obtained with Dropsens' commercial gold SPEs, which have a diameter of 4 mm as opposed to the manufactured electrodes' diameter of 3 mm, however, the *S*a/*S*g ratio achieved with the commercial electrodes in the same conditions was 5.76, which is a strong indication of the high performance of the electrodes produced in the polyimide membrane.

3.3 Biosensor assembly for IL-6 detection

3.3.1 Optimization of the electrode performance

During the fabrication of MIP-based materials, different approaches can be explored to provide the more suitable detection features like sensitivity, reproducibility and detection limits. Herein, surface imprinting approach was chosen. The entire biosensor construction process can be summarized in the schematic below (Figure 6).

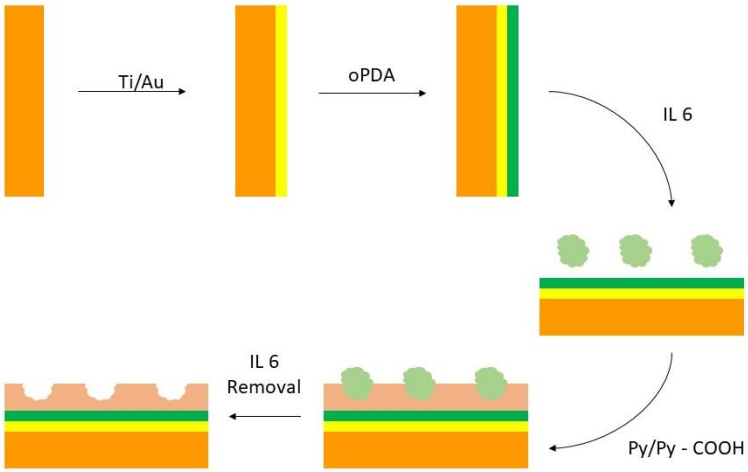

Figure 6 - Biosensor fabrication schematic.

One of the main goals during the development of a biosensor is to obtain reproducible results; thus, cleaning the electrode surface is naturally the first and a critical step to achieve a good performance. The implementation of this pre-treatment stage eliminates some problems, such as, the lack of reproducibility and surface contamination, which ensures a better and more consistent point of departure for the fabrication of the imprinted polymer. Two approaches were tried in this context: (1) washing with an ethanolic solution (99%), followed by washing with Millipore water and drying with a nitrogen jet; and (2) electrochemical cleaning with a solution of 0.5 M H_2S0_4 solution (scan-rate of 50 mV/s, potential range of -0.2 V to +1.2 V, and 5 sweep cycles), followed by washing with Millipore water and drying with a nitrogen jet.

EIS measurements were performed to follow-up the variation of the gold-modified electrodes after each chemical modification since this electrochemical technique holds a high sensitivity without causing a significant perturbation in the system. It was observed that both cleaning approaches caused a decrease of *R*ct making the gold electrode surfaces more conductive. Electrochemical cleaning with sulphuric acid was chosen as the more suitable cleaning procedure because it enabled electrochemical measurements with higher stability and reproducibility (Figure 7a).

After cleaning the transducer surface, the next step was to perform the physical adsorption of the target protein (IL-6), followed by the electrical polymerization of the monomers. After incubating the protein on the WE at room temperature for 3 hours, it was observed that the presence of the IL-6 on the gold surface caused an increase of the *R*ct (Figure 7b), as expected. Then, the electropolymerization of two functional monomers, EDOT and Py was carried in-situ, in order to create a polymeric film around the protein (Figure 7c). As displayed in Figure 7d, the electropolymerization of EDOT and Py monomers resulted in a substantial increase of impedance due to the blocking of electron transfer by the polymeric matrix. The selected functional monomers were EDOT and Py due to its good conductivity and electrochemical stability, while the concentration ratio of 5:1 was already tested in previous works that had already been performed [45]. The assembly of the MIP was subsequently completed by removing the protein and leaving the cavities available for the rebinding event (Figure 7e). Herein, the removal of the template was achieved by incubating only in the WE a solution of H_2SO_4 0.5 M for two hours. This procedure has led to a substantial *R*ct decrease of both NIP and MIP films. The analytical performance of the biosensing material was then evaluated by recording calibration curves that were obtained after incubation of increasing concentration solutions of IL-6 in the WE. The results obtained showed that the resistance of the sensing layer increased after incubating an IL-6 solution in the MIP film, which could be due to the re-binding of the protein molecule onto the imprinted cavities that hindered the electrical features of the sensing surface. By looking to Figure 7f, it can be seen the calibration curves plotted with the (relative) *R*ct of MIP and NIP sensors against the logarithm concentration of IL-6. Although the MIP seems to display a more linear behaviour, in comparison with the NIP, the sensitivity of the response is quite low and needs further improvement.

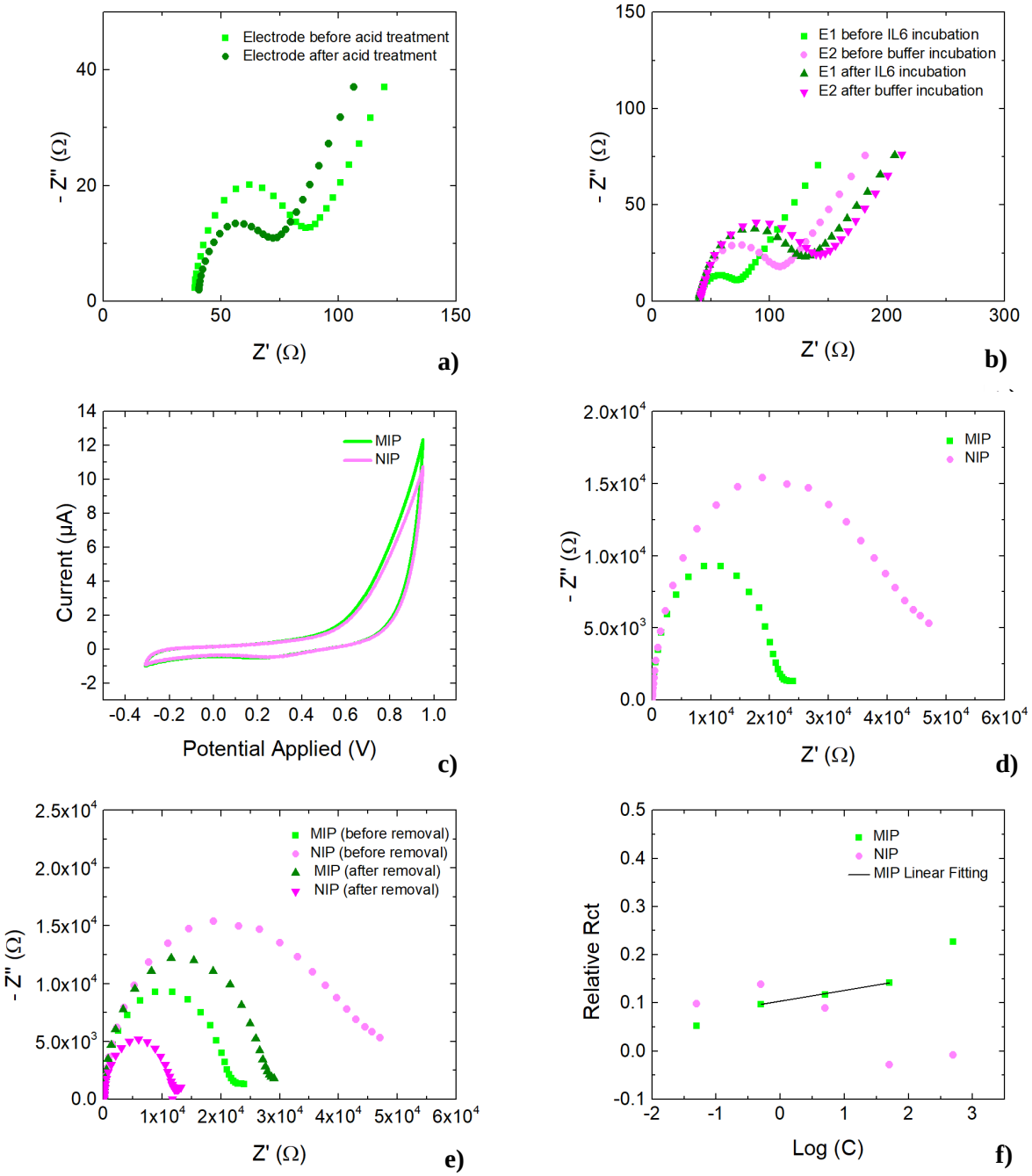

Figure 7 - a) Electrodes before and after cleaning; b) Electrodes before and after IL-6 or buffer incubation; c) CV during electropolymerization of MIP and NIP; d) EIS data regarding MIP and NIP after electropolymerization; e) EIS data before and after removal; f) Calibration curve regarding MIP and NIP

3.3.1.1 Surface functionalization with ortho-phenylenediamine (o-PDA)

In order to promote a higher and more oriented binding of the protein to the gold surface, it was important to functionalize the surface. For this purpose, o-PDA was chosen because it is an electroactive monomer with amine functional groups connected to an aromatic ring that can facilitate the protein binding [46]. The electropolymerization of o-PDA was carried out for one cycle, to avoid high impedimetric behaviour, at a scan-rate of 150 mV/s in the potential range of -0.2 V to +1 V. Along this study, two concentrations were tested of this monomer: 5 mM and 0.5 mM.

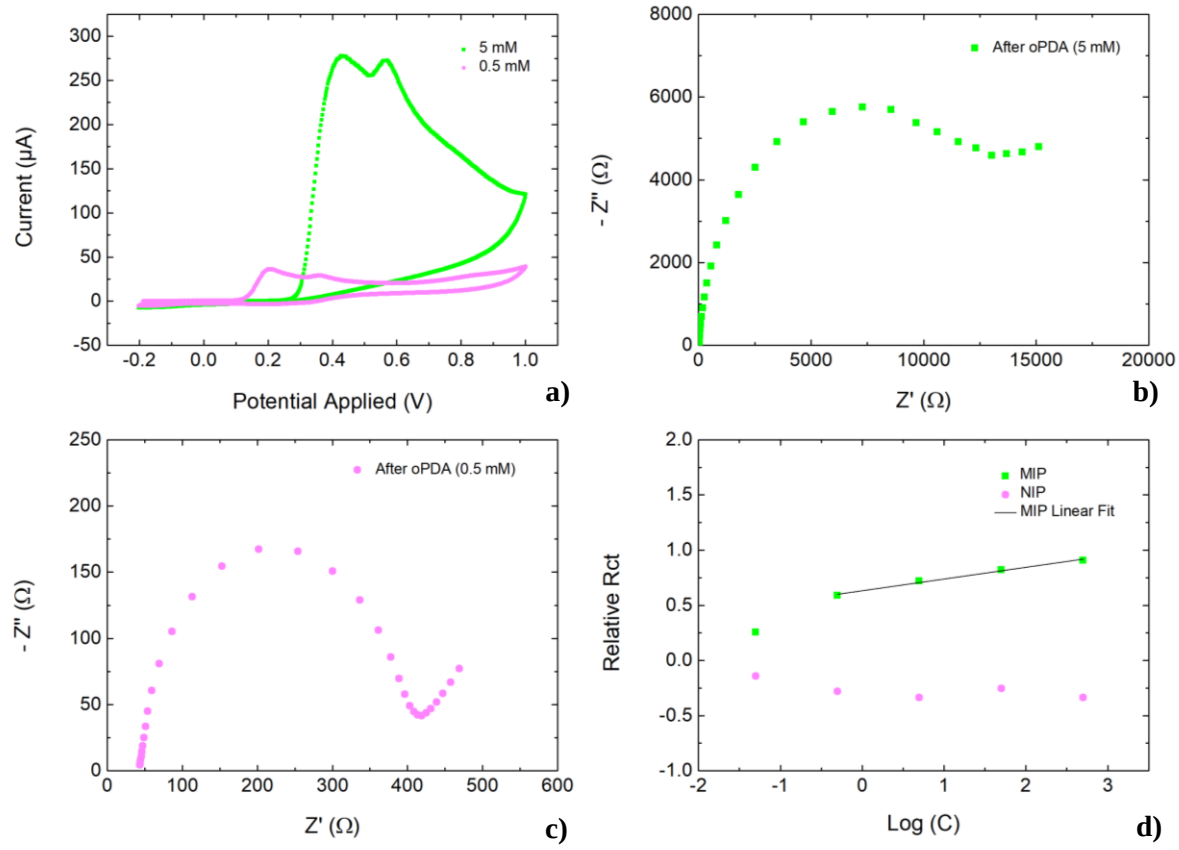

Figure 8 - a) Electropolymerization of o-PDA by means of CV; b) EIS data after 5 mM o-PDA electropolymerization; c) EIS data after 0.5 mM electropolymerization; d) Calibration curve regarding MIP and NIP fabricated with a layer of 0.5 mM p(o-PDA).

As seen in the Figure 8a, the typical oxidation peak of o-PDA appeared at +0.2 V for the concentration of 0.5 mM while for the higher concentration the peak moved for higher potential values at +0.4 V [47]. It was observed an increase of the *R*ct values after electropolymerizations of the two o-PDA concentrations, with the highest increase corresponding to the 5 mM concentration, which is the result of the formation of a less conductive polymeric matrix (Figure 8b-c). Due to the strong insulating effect obtained with the higher concentration, 0.5 mM was selected as the optimum phenol concentration because it seems sufficient to functionalize the surface. Then, the imprinted material was assembled by using the previous mixture of EDOT and Py monomers, in the same conditions. Furthermore, as shown in the Figure 8d, when the biosensor assembled with the concentration of 0.5 mM of o-PDA was calibrated, the MIP exhibited a linear behaviour with increasing analyte concentration while the NIP exhibited no linear response.

3.3.1.2 Effect of the number of cycles during electropolymerization

During the growth of the polymer around the protein template is especially important to control the thickness of the film, particularly regarding MIPs obtained through a surface imprinting approach in order to avoid the complete entrapment of the protein. So, the polymerization process must be carefully optimized to produce a stable, controlled, and effective polymer.

The electropolymerization so far had been carried out in the potential range of -0.3 V to +0.95 V at a scan-rate of 50 mV/s and for 5 cycles. However, given that the experimental results were not reproducible, the next

step was to decrease the number of cycles to 3, because with 5 cycles of electropolymerization, the polymer could become too thick with fewer imprinted sites exposed, significantly reducing the sensitivity.

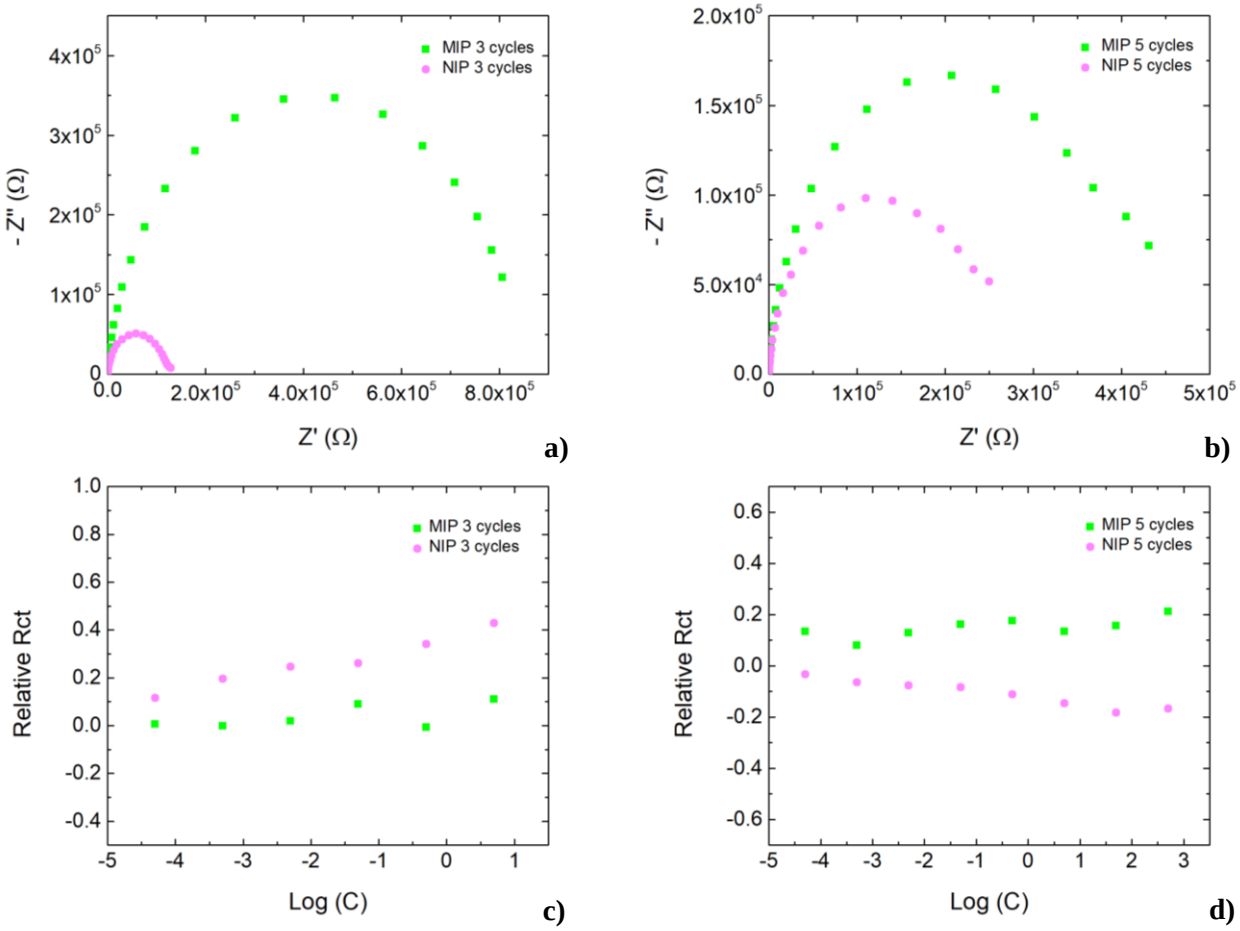

Figure 9 -a) Nyquist plots for NIP and MIP after 3 cycles of electropolymerization;b) Nyquist plots for NIP and MIP after 5 cycles of electropolymerization; c) Calibration curves of MIP/NIP with 3 cycles of polymerization; d) Calibration curves of MIP/NIP with 5 cycles of electropolymerization.

After electropolymerization, it was observed a substantial increase of the *R*ct values for all electrodes. Like expected, the 3-cycle NIP presented a lower Rct value than the 5-cycle NIP, while the corresponding MIPs displayed an opposite behaviour (Figure 9a-b). It was foreseen that by increasing the number of cycles during the polymerization, more polymer with higher thickness could be formed and so, NIP with 5 cycles would be more insulating than the NIP with 3 cycles. The opposite behaviour observed with the MIPs can be explained by the effect caused with the presence of the protein entrapped within the polymeric matrix, that also can inhibit the growth of the polymeric film.

To remove the template protein, it is essential to choose an effective method that does not degrade or modify the polymeric film, leaving the imprinting sites free for analyte recognition [48]. In parallel, the NIP control is manufactured in the same conditions but without the protein because the effect of this removal solutions on the polymer itself needs to be also investigated. One of the first methods tested along this work was the incubation of the modified electrodes in an acidic solution for 1h. Although the previous results looked promising, the calibrations were not yet ideal (lack of sensitivity and reproducibility) and so, the next step was to change the removal approach by maintaining an incubation in sulphuric acid solution (0.5 M, 2 h) followed

by an electrochemical removal by means of CV. It is expected that this process will change the porosity of the polymer mesh in order to release the imprinted protein as well as remove other monomer residues that did not polymerize. During this removal step, the sensor was treated by CV, for 3 cycles, up to a scan-rate of 50 mV/s, in pH 7.4 phosphate buffer and to 2 different potential ranges were tested: from -0.3 V to +0.3 V and from -0.3 V to +0.95 V (the same used for the polymerization), being the last option more effective in achieving a better linear response for MIP sensor.

In terms of calibration, it was observed that decreasing the number of cycles during the electropolymerization do not improve the response of the MIP sensor (Figure 9c). In contrast with the 3-cycle NIP, the 5-cycle NIP does not seem to respond to the increasing concentrations of IL-6 (Figure 9d), and thus, we proceeded with a 5 cycle electropolymerization as this allows a control sample that does not show a linear response as a result of non-specific bonding.

3.3.1.3 The influence of the pH

Looking carefully to the calibration assays, it was noted that the electrochemical response of the MIP-based sensor still needed to be improved and so, the pH of the phosphate buffer solution was reduced from 7.4 to 5.8, in order to change the charge distribution and work closer to the protein's isoelectric point, pI ~6.2, (reference Abcam ab9627, MW 21 kDa, 29-212 amino acids) [49], [50]. Keeping the other optimized experimental conditions, the calibrations were repeated, but yet no improvement was obtained.

So, the next step was to lower the pH once again, this time to 4.8, to get further away to the protein's pI. Herein, the goal was to work with the protein at a predominantly positive charge. In this condition, the protein becomes more protonated, with a positive charge, which can enhance some electrostatic interactions with the polymer. At this pH, the removal step vas performed by incubating the sample in acid for 2h followed by electrochemical removal by CV, as before (Figure 10a). As displayed, the MIP sensor demonstrated a better and linear response to the successive incubations of the protein over the range 5 pg/mL and 50 ng/mL (Figure 10b), however more experiments have showed that this system is not yet reproducible, which can be due to the nature of the selected polymers.

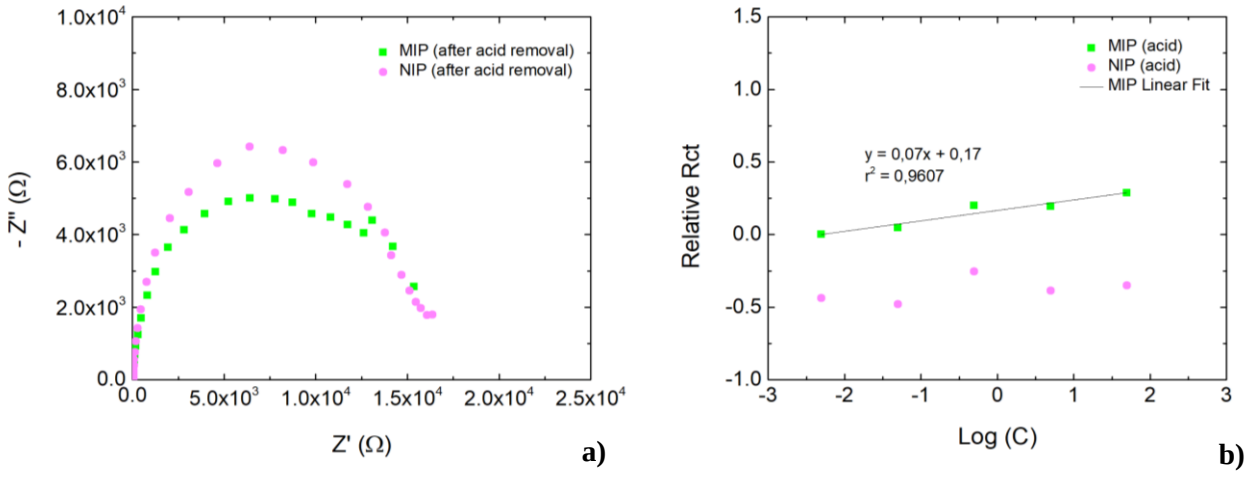

Figure 10 - a) EIS data regarding MIP and NIP sensors after the removal step; b) Calibration curves of MIP and NIP sensors.

3.3.1.4 Effect of the monomer interactions

Although the previous results seem to enable a positive response regarding the MIP calibration, the next focus was to test other monomers in order to strengthen the affinity between the protein and the polymer. It is known that both EDOT and Py lack a functional group that can benefit this type of interaction so, EDOT was replaced by Py-COOH, which has a carboxyl group and a pKa value of 5 [51].

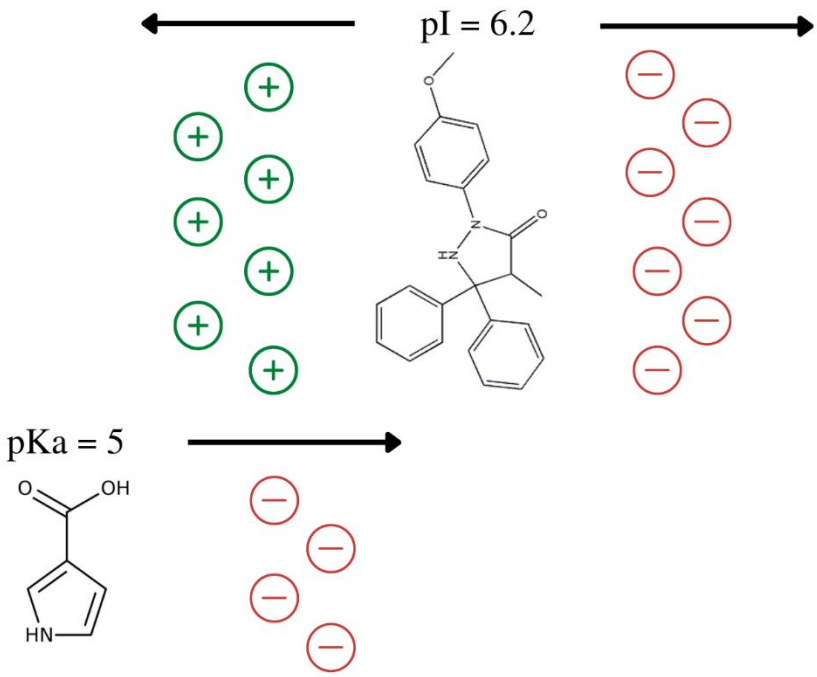

Figure 11- Schematic of charge distribution for IL-6 and Py-COOH structures according to pH variation.

With the purpose of taking advantage of electrostatic interactions between the protein target and the polymeric environment, an ideal pH range of 5 to 6 seems to promote higher affinity between protonated IL-6 (positive) and deprotonated Py-COOH (negative) (Figure 11) [52]. Thus, 4 electropolymerization cycles were performed at two pH values: 5.8 and 4.8 (Figure 12a-b).

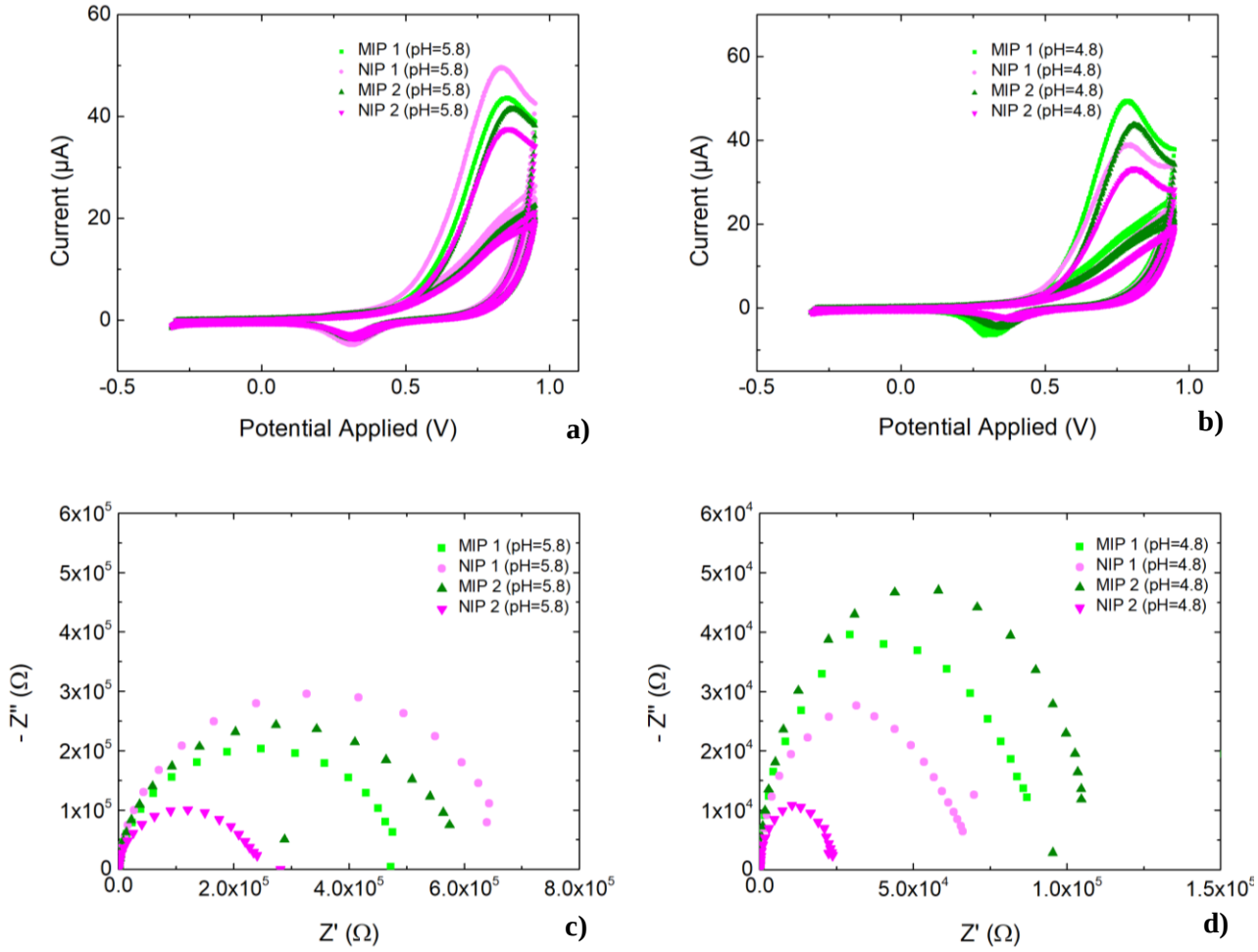

Figure 12 - a) CVs regarding electropolymerization at a 5.8 pH; b) CVs regarding electropolymerization at a 4.8 pH; c) EIS data for MIPs and NIPs after electropolymerization in a 5.8 pH; d) EIS data for MIPs and NIPs after electropolymerization in a 4.8 pH

All tests were performed in duplicate to investigate the reproducibility throughout the biosensor assembly. As can be seen in the graphs above, at a pH of 5.8 we did not have consistent results, since one of the NIPs has the highest resistance while the other has the lowest, and the resistances of the MIPs are between these two values (Figure 12c). Regarding the assay at pH of 4.8, it is possible to verify that both MIPs presented higher resistances in comparison with the NIP ones, which can result from the presence of the protein entrapped in the polymeric matrix and so, causing a higher obstacle to the passage of electrons (Figure 12d). According to these results, a mixture of Py and Py-COOH prepared at a pH of 4.8 (near 5) seems to be the optimal condition for MIP assembly.

3.3.2 Characterization of the MIP film

3.3.2.1 XPS analysis

Regarding the characterization of the biosensor, five samples were evaluated by X-ray photoelectron spectroscopy (XPS) to draw conclusions about protocol optimizations.

XPS is a surface characterization technique used to provide information about a material's elemental composition and binding states. The XPS study was performed by exposing the samples to X-rays and measuring the kinetic energy of electrons emitted from the top (from 1 to 10 nm) of the material under study. Surface atoms contain characteristic peaks, the energy and intensity of which allow identification and quantification of all surface elements present (except hydrogen) [53]. The first sample was the electrode with nothing on the surface to determine the starting point, followed by a sample with IL-6 to determine whether it was adsorbed or if adding a functional layer of o-PDA would be beneficial. In order to detect the presence of the polymer and protein, a MIP/NIP pair with an o-PDA functional layer and only an EDOT/Py polymer layer was also studied. A MIP treated with acid removal was also analysed to draw conclusions regarding the removal process.

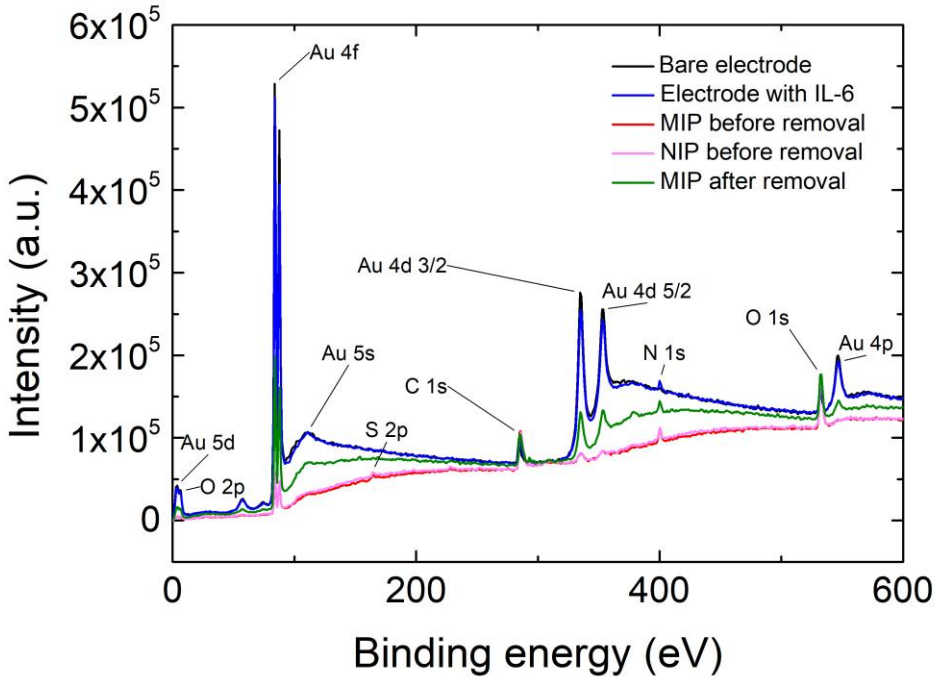

Figure 13 - XPS analysis of the biosensor along the different stages of electrode modification.

As we can observe in Figure 13, gold is a common element in all samples because it is used to produce the electrodes; but, as we build the biosensor, it is no longer as concentrated on the surface, resulting in a decrease in characteristic peaks in samples that already have the polymer layer.

Regarding the sample after incubation of the protein, the same intensity of the oxygen, carbon and nitrogen peaks was verified as the sample without the protein, which is a strong indication that very few (or almost none) protein is adsorbed to the surface, hence the functional layer of poly(o-PDA). As for the MIP/NIP before removal, this pair exhibits the expected sulfur and nitrogen peaks, confirming that electropolymerization of the EDOT/Py mixture was effective. However, there was no difference between these two regarding the peaks that could identify the protein, which can be explained by the similar elementary composition of these organic materials. Also, the polymer is present in a much higher proportion in comparison with the IL-6 protein, resulting in a predominant effect.

Comparing the MIPs before and after removal, we were able to detect a slight decrease in nitrogen and sulfur peaks and, with more gold detected in the latter MIP, which suggests that this process may be responsible for also removing parts of the polymer (and unreacted monomers), leaving the gold material more exposed on the surface.

3.3.2.2 FTIR analysis

Samples were analysed for each step: bare gold electrode, a functional layer of poly(o-PDA), a functional layer of poly(o-PDA) with IL-6 protein deposition, and a MIP and NIP sensors, assembled with 3 electropolymerization cycles of Py and Py-COOH monomers.

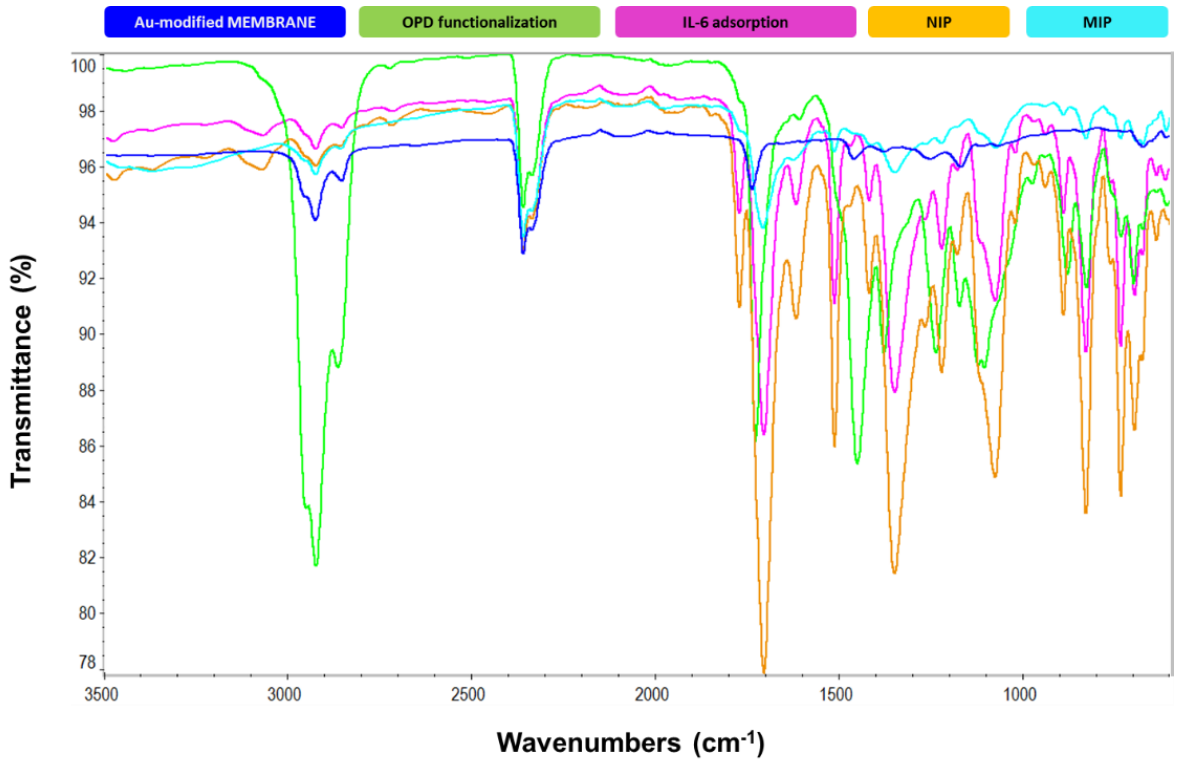

Figure 14 – ATR-FTIR spectra regarding each modification step along biosensor fabrication

The ATR-FTIR spectrum (Figure 14) of the sample with the poly(o-PDA) layer is characterized by main bands at, approximately, 700 cm^{-1} and 1100 cm^{-1} which could be attributed to out of plane deformation of CH for 1,2-disubstituted benzene and 1,2,4 tri-substituted of benzene ring. The sharp absorption band that appears at 1350 cm^{-1} could be attributed to symmetric stretching vibration of C–N (aromatic amine). The sharp absorption band appearing at around 1700 cm−1 which may be attributed to N-H deformation of secondary amine, deformation of the benzene ring. The shoulder absorption band that appears around 3000 cm^{-1} can be attributed to the symmetrical stretching vibration of C-H in the aromatic ring which should disappear after polymerization, which means that not all the monomer has polymerized [54].

The spectrum after protein adsorption presented the main region: the region of amide I and amide II that gives information about the protein content and its secondary structure. These bands can be observed in the regions 1600–1700 cm^{-1} and 1480–1600 cm^{-1}, respectively. Amide I peak due to stretching vibration of C=O was seen at 1700 cm^{-1}, and Amide II peaks derived mainly from in-plane N-H bending are observed at 1512 cm^{-1} [55], [56]. These amide bands proved the immobilization of IL-6 to poly(o-PDA) functional groups. C-N stretch of aliphatic amines is also observed at 1076 cm^{-1} and the rest of the bands are derived mainly from CH_2 rocking vibration [57].

No substantial differences could be verified on the FTIR spectra of NIP and MIP materials besides a small band around 3100 cm^{-1} that is present in both MIP and IL-6 modified sample that can be assigned to the stretching vibrations of -OH and -NH, proving the presence of the protein.

3.3.2.3 SEM analysis

Scanning electron microscopy (SEM) was employed to morphologically characterize the biosensor as it is one of the most common methods for obtaining images of microstructures. A low-energy electron beam is emitted into the material and sweeps across the surface of the sample. As the beam approaches and enters the material, many interactions occur, resulting in the emission of photons and electrons from or near the surface of the sample [58]. Samples were analysed for each step: bare electrodes sample, sample with gold and functional layer of poly(o-PDA), sample with gold, functional layer of poly(o-PDA) and IL-6 protein. As for MIP and NIP samples, it was used 3 electropolymerization cycles of Py and Py-COOH monomers.

According with the Figure 15a, from the bare gold electrodes image it was possible to observe a quite homogeneous distribution of the gold that was deposited by e-beam. When the functional layer of poly(o-PDA) was applied (Figure 15b), we obtained a different and more uniform morphology, which proves the uniform polymer growth.

After adding the protein under study (Figure 15c), it was possible to observe that the surface seems more heterogenous in contrast to the previous polymer's uniform layer and, interestingly, the image seems less bright and clean, which can stand as an indication that a less conductive surface was obtained after the adsorption of the protein structure. Looking to the MIP and NIP (Figure 15d and Figure 15e) images, an obvious morphological modification is observed in comparison with previous poly(o-PDA) layer. The surfaces seem less organized, and, in both samples, it was possible to verify the uniform distribution of the polymer grown by electropolymerization.

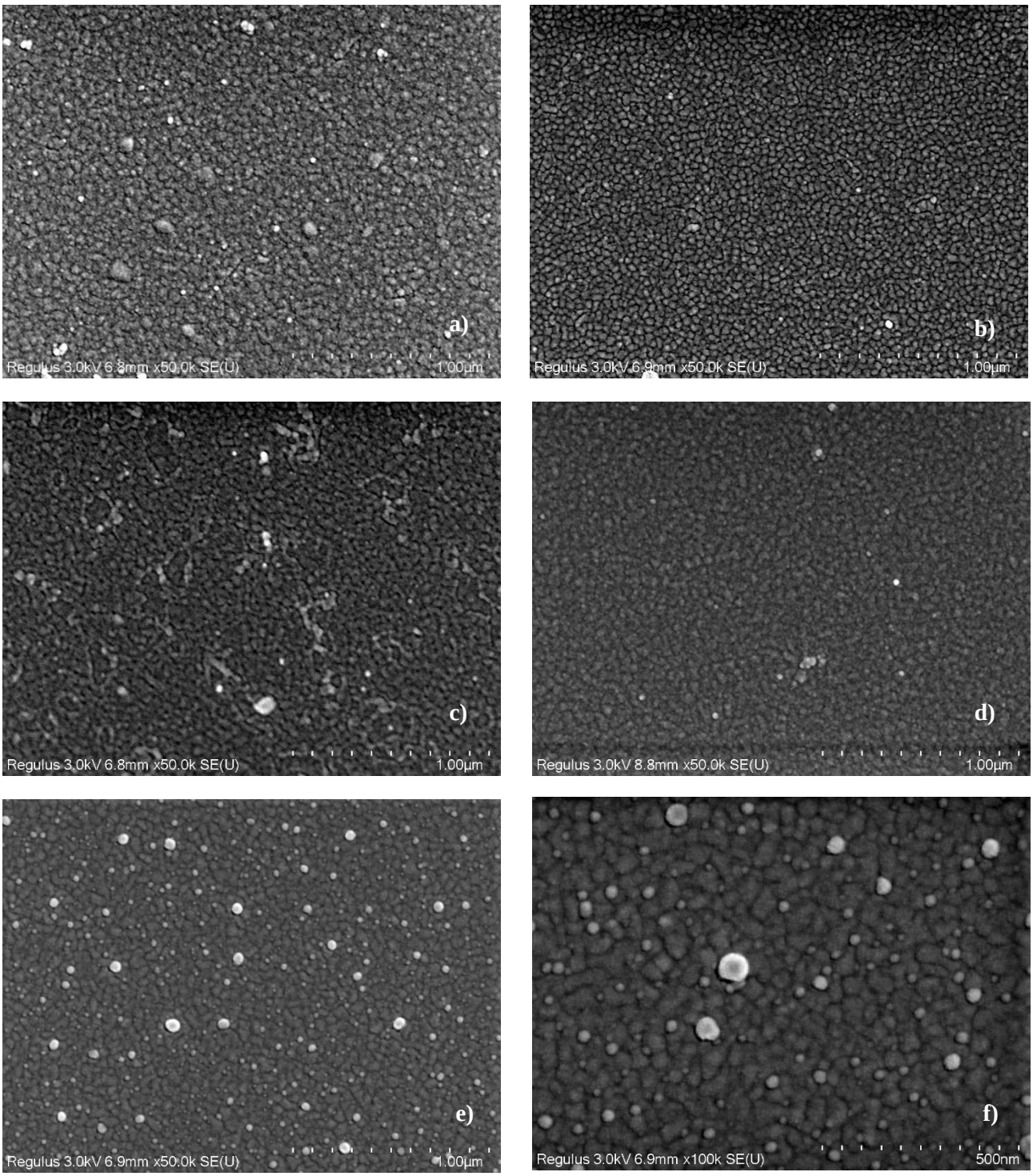

Figure 15 - SEM analysis of: a) bare gold electrodes sample; b) sample with gold and functional layer of poly(o-PDA); c) sample with gold, functional layer of poly(o-PDA) and IL-6 protein; d) NIP; e) MIP; f) MIP zoomed in;

3.3.3 Analytical performance of the (bio)sensor

After optimizing the more suitable parameters of the biosensor assembly, the analytical performance of IL-6 sensory materials prepared at a pH of 4.8 using Py and Py-COOH monomers was evaluated by recording calibration curves with DPV technique, instead of EIS. The choice of this voltammetric approach to be used as the electrochemical detection technique was due to it being more sensitive to small variations. Initially, it was observed that after successive incubations of IL-6 protein solutions, both the MIP and the NIP exhibited an electrochemical response with increasing protein concentrations. This result seems to indicate that, in these conditions, the polymeric film fabricated in the surface of the electrodes can promote some non-specific binding of the protein. This means that the affinity between the protein and the polymer layer is quite strong, regardless of the production of the cavities. So, in order to reduce this undesirable effect, the number of cycles during the electropolymerization was reduced from 4 to 3. The goal here was to create a thinner layer of polymer and therefore reduce the non-specific interactions at the surface of the polymer.

Regarding the removal of the imprinted protein, since we are working at a more acidic pH, the method chosen for this purpose has been an incubation in 0.1 M NaOH, a basic solution, for one hour, followed by incubation in citrate buffer to stabilize the pH.

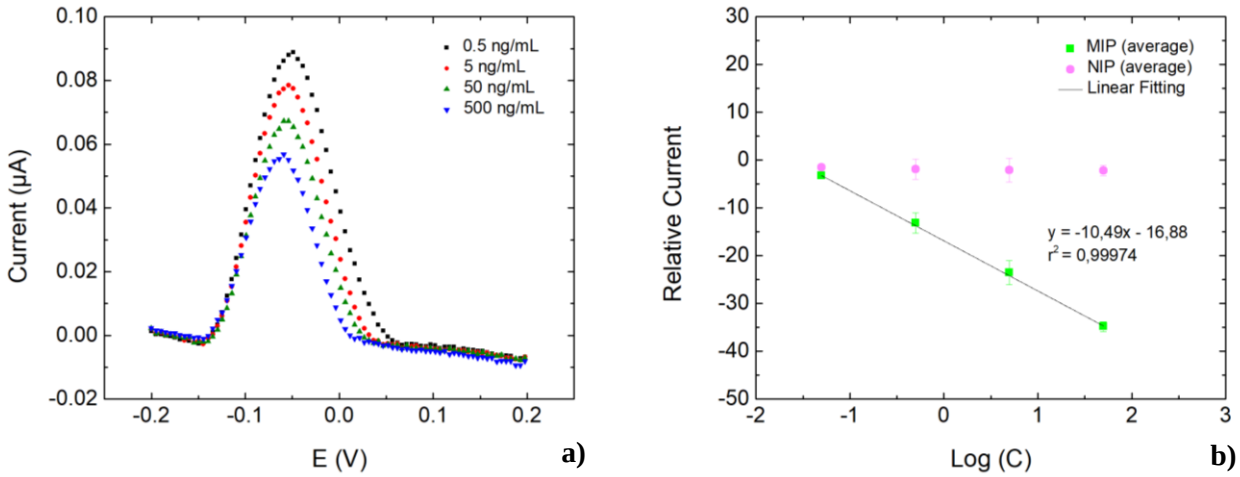

Figure 16 - a) DPV recordings for each standard concentration of a MIP; b) MIP and NIP calibration curve with error bars

So, after biosensor assembly in the optimized conditions, the final calibrations of both MIP and NIP are presented in Figure 16. As expected, the peak current decreased as the IL-6 protein concentration was increased, as a result of the occupation of the cavity sites in the MIP film by the protein target, blocking the diffusion of the $Fe(CN)_6^{3-/4-}$ probe. These tests were performed in duplicate so, good reproducibility can be proven by the error bars present in the graphs. Furthermore, the developed biosensor presented a good response over the concentration range of 0.5 - 500 ng/ mL, while the control NIP does not respond.

Homeostatic production of IL-6 results in levels ranging from 1 pg/ml to 10 pg/ml [59], but these can increase to the nanograms/ml range during inflammation, however, when consulting the literature, it was not possible reach a conclusive cut-off value, with values such as 35 pg/mL [60], 86 pg/mL[61] or even 200 pg/mL [62] being presented, which means that there is still no defined and equal value for all people regarding the cut-off with/without inflammation. Although more sensitive sensing devices for IL-6 detection can be found in the literature, most of them are using conventional rigid platforms that cannot be applied for wearable sensing. As a result, the proposed flexible biosensor acts in the area of interest for its application.

4
CONCLUSION AND FUTURE PERSPECTIVES

The primary goal of this work, which was to produce conformable electrochemical biosensors for wound monitoring using polymeric membranes made in CENIMAT laboratory, was successfully achieved. The usage of these membranes has a significant advantage since the polymeric substrate can be manufactured to meet precise requirements and specifications such as thickness, mechanical and electrical qualities. The produced membranes presented a thickness of 6 µm and allowed the deposition of a high controlled nanolayer of gold conductive material. After this manufacturing process, the modified membranes can be safely attached to the skin due to their biocompatibility and excellent mechanical stability.

The main motivation of this work was to develop an electrochemical biosensor with good flexibility and reproducibility characteristics to be used in the context of wound inflammation monitoring. In particular, an inflammatory biomarker, interleukin 6. (IL-6) was selected as the target molecule. The recognition element was produced by molecular imprinting technology, which has various advantages over natural antibodies in terms of chemical stability, overall ease of manufacture, and low production costs.

Along the biosensor assembly, important parameters like electrode functionalization and type of monomers for electropolymerization were investigated in order to generate a polymeric matrix holding functional groups that increased the affinity between the polymer and protein. The best parameters for electropolymerization included a potential range of [-0.3; +0.95] V for 3 cycles at a scan-rate of 150 mV/s. The process of removing IL-6 from the polymer matrix was also optimized using a solvent that should not induce a substantial modification or degradation of the NIP material. Removal was performed by incubating NaOH solution in the WE surface followed by incubation in buffer to regulate pH.

The XPS analysis during the optimization of these parameters demonstrated the need for the functional layer of o-PDA, since it demonstrated that the protein did not adsorb to the surface of the electrodes, and also showed that the removal with sulfuric acid was not the most indicated since removed part of the polymer, eventually affecting the formation of cavities for rebinding. Thus, this characterization helped to choose the best conditions for electropolymerization and removal, as well as the monomers used. In addition, SEM and FTIR analysis were also valuable techniques used to follow and attest the modifications on each step of the biosensor fabrication. Both techniques presented subtle differences between NIP and MIP sensors which is an indication of the protein presence during the MIP growth.

In addition, it was also necessary to study the influence of pH on the construction of the biosensor, which played a great role in the balance of charges. The final value chosen turned out to be 4.8, in order to work with the protein in its positive form and thus increase the affinity with the polymer matrix.

Overall, the MIP-based sensor showed good electrochemical response, in the IL-6 concentration range of 0.5 ng/mL to 500 ng/mL, good reproducibility, quick response time (30 min of incubation) and stability, in addition to being the first MIP developed in a flexible substrate for IL-6 detection. Although the ideal concentration range of IL-6 in biological samples is around picoMolar, the herein proposed sensor can be in the future improved by the incorporation of nanomaterials that can greatly enhance the sensitivity of the electrochemical response. Nevertheless, in order to determine the LOD of this technique more calibrations in buffer are still needed.

This promising new approach opens the way for the rapid diagnosis of biomarkers associated with inflammation in an accurate and minimally invasive manner. As a future perspective, it would also be

important to carry out tests on real human samples (or interferent assays) to evaluate the selectivity features of the developed biosensor and make a comparison of this method with another validated method.

REFERENCES

[1] H. Derakhshandeh, S. S. Kashaf, F. Aghabaglou, I. O. Ghanavati, and A. Tamayol, "Smart Bandages: The Future of Wound Care," *Trends in Biotechnology*, vol. 36, no. 12. Elsevier Ltd, pp. 1259–1274, Dec. 01, 2018. doi: 10.1016/j.tibtech.2018.07.007.

[2] E. Gianino, C. Miller, and J. Gilmore, "Smart Wound Dressings for Diabetic Chronic Wounds," *Bioengineering (Basel)*, vol. 5, no. 3, Sep. 2018, doi: 10.3390/BIOENGINEERING5030051.

[3] M. S. Brown, B. Ashley, and A. Koh, "Wearable Technology for Chronic Wound Monitoring: Current Dressings, Advancements, and Future Prospects," *Front Bioeng Biotechnol*, vol. 6, no. APR, Apr. 2018, doi: 10.3389/FBIOE.2018.00047.

[4] T. R. Dargaville, B. L. Farrugia, J. A. Broadbent, S. Pace, Z. Upton, and N. H. Voelcker, "Sensors and imaging for wound healing: a review," *Biosens Bioelectron*, vol. 41, no. 1, pp. 30–42, Mar. 2013, doi: 10.1016/J.BIOS.2012.09.029.

[5] M. Ochoa, R. Rahimi, and B. Ziaie, "Flexible sensors for chronic wound management," *IEEE Rev Biomed Eng*, vol. 7, pp. 73–86, 2014, doi: 10.1109/RBME.2013.2295817.

[6] A. U. Ahmed, "An overview of inflammation: Mechanism and consequences," *Frontiers of Biology in China*, vol. 6, no. 4. pp. 274–281, Aug. 2011. doi: 10.1007/s11515-011-1123-9.

[7] G. Zhao et al., "Biofilms and Inflammation in Chronic Wounds," *Adv Wound Care (New Rochelle)*, vol. 2, no. 7, pp. 389–399, Sep. 2013, doi: 10.1089/wound.2012.0381.

[8] S. Kany, J. T. Vollrath, and B. Relja, "Cytokines in inflammatory disease," *International Journal of Molecular Sciences*, vol. 20, no. 23. MDPI AG, Dec. 01, 2019. doi: 10.3390/ijms20236008.

[9] W. Lohcharoenkal, Z. Abbas, and Y. Rojanasakul, "Advances in nanotechnology-based biosensing of immunoregulatory cytokines," *Biosensors*, vol. 11, no. 10. MDPI, Oct. 01, 2021. doi: 10.3390/bios11100364.

[10] T. Hirano, "IL-6 in inflammation, autoimmunity and cancer," *International immunology*, vol. 33, no. 3. NLM (Medline), pp. 127–148, Mar. 01, 2021. doi: 10.1093/intimm/dxaa078.

[11] Y. Liu, H. Qing, and Y. Deng, "Biomarkers in Alzheimer's disease analysis by mass spectrometry-based proteomics," *Int J Mol Sci*, vol. 15, no. 5, pp. 7865–7882, May 2014, doi: 10.3390/IJMS15057865.

[12] H. Kalish and T. M. Phillips, "Application of immunoaffinity capillary electrophoresis to the measurements of secreted cytokines by cultured astrocytes," *J Sep Sci*, vol. 32, no. 10, p. 1605, May 2009, doi: 10.1002/JSSC.200900047.

[13] S. Ye, S. Feng, L. Huang, and S. Bian, "Recent Progress in Wearable Biosensors: From Healthcare Monitoring to Sports Analytics," *Biosensors 2020*, vol. 10, no. 12, p. 205, Dec. 2020, doi: 10.3390/BIOS10120205.

[14] A. Haleem, M. Javaid, R. P. Singh, R. Suman, and S. Rab, "Biosensors applications in medical field: A brief review," *Sensors International*, vol. 2, p. 100100, Jan. 2021, doi: 10.1016/J.SINTL.2021.100100.

[15] N. Bhalla, P. Jolly, N. Formisano, and P. Estrela, "Introduction to biosensors," *Essays Biochem*, vol. 60, no. 1, p. 1, Jun. 2016, doi: 10.1042/EBC20150001.

[16] V. Naresh and N. Lee, "A review on biosensors and recent development of nanostructured materials-enabled biosensors," *Sensors (Switzerland)*, vol. 21, no. 4. MDPI AG, pp. 1–35, Feb. 02, 2021. doi: 10.3390/s21041109.

[17] H. A. Alhadrami, "Biosensors: Classifications, medical applications, and future prospective," *Biotechnol Appl Biochem*, vol. 65, no. 3, pp. 497–508, May 2018, doi: 10.1002/BAB.1621.

[18] M. Cieplak and W. Kutner, "Artificial Biosensors: How Can Molecular Imprinting Mimic Biorecognition?," *Trends in Biotechnology*, vol. 34, no. 11. Elsevier Ltd, pp. 922–941, Nov. 01, 2016. doi: 10.1016/j.tibtech.2016.05.011.

[19] O. I. Parisi et al., “The Evolution of Molecular Recognition: From Antibodies to Molecularly Imprinted Polymers (MIPs) as Artificial Counterpart,” *Journal of Functional Biomaterials*, vol. 13, no. 1. MDPI, Mar. 01, 2022. doi: 10.3390/jfb13010012.

[20] A. A. Ensafi, N. Kazemifard, and H. R. Jamei, “Molecularly imprinted biosensors for sensitive detection of biomarkers,” in *The Detection of Biomarkers*, Elsevier, 2022, pp. 435–456. doi: 10.1016/b978-0-12-822859-3.00019-5.

[21] M. F. Frasco, L. A. A. N. A. Truta, M. G. F. Sales, and F. T. C. Moreira, “Imprinting technology in electrochemical biomimetic sensors,” *Sensors (Switzerland)*, vol. 17, no. 3. MDPI AG, Mar. 06, 2017. doi: 10.3390/s17030523.

[22] P. T. Kissinger and W. R. Heineman, “Cyclic voltammetry,” *J Chem Educ*, vol. 60, no. 9, pp. 702–706, 1983, doi: 10.1021/ED060P702.

[23] L. A. de Carvalho, A. R. de Andrade, and P. R. Bueno, “Espectroscopia de impedância eletroquímica aplicada ao estudo das reações heterogêneas em ânodos dimensionalmente estáveis,” *SciELO*, vol. 29, no. 4, pp. 796–804, Jul. 2006, doi: 10.1590/S0100-40422006000400029.

[24] H. S. Magar, R. Y. A. Hassan, and A. Mulchandani, “Electrochemical Impedance Spectroscopy (EIS): Principles, Construction, and Biosensing Applications,” *Sensors 2021*, Vol. 21, Page 6578, vol. 21, no. 19, p. 6578, Oct. 2021, doi: 10.3390/S21196578.

[25] M. de L. Gonçalves, L. A. N. Truta, M. G. F. Sales, and F. T. C. Moreira, “Electrochemical Point-of Care (PoC) Determination of Interleukin-6 (IL-6) Using a Pyrrole (Py) Molecularly Imprinted Polymer (MIP) on a Carbon-Screen Printed Electrode (C-SPE),” *Anal Lett*, vol. 54, no. 16, pp. 2611–2623, 2021, doi: 10.1080/00032719.2021.1879108.

[26] N. Özcan, C. Karaman, N. Atar, O. Karaman, and M. L. Yola, “A Novel Molecularly Imprinting Biosensor Including Graphene Quantum Dots/Multi-Walled Carbon Nanotubes Composite for Interleukin-6 Detection and Electrochemical Biosensor Validation,” *ECS Journal of Solid State Science and Technology*, vol. 9, no. 12, p. 121010, Dec. 2020, doi: 10.1149/2162-8777/abd149.

[27] Kenry, J. C. Yeo, and C. T. Lim, “Emerging flexible and wearable physical sensing platforms for healthcare and biomedical applications,” *Microsyst Nanoeng*, vol. 2, no. October 2015, 2016, doi: 10.1038/micronano.2016.43.

[28] J. Kim, A. S. Campbell, B. E. F. de Ávila, and J. Wang, “Wearable biosensors for healthcare monitoring,” *Nature Biotechnology* 2019 37:4, vol. 37, no. 4, pp. 389–406, Feb. 2019, doi: 10.1038/s41587-019-0045-y.

[29] L. B. Rothman, “Properties of Thin Polyimide Films,” *J Electrochem Soc*, vol. 127, no. 10, pp. 2216–2220, Oct. 1980, doi: 10.1149/1.2129377/XML.

[30] J. A. Kreuz and J. R. Edman, “Polyimide Films.”, *Adv. Mater.*, vol.10, pp. 1229-1232, 1998, doi: 10.1002/(SICI)1521-4095(199810)10:15<1229::AID-ADMA1229>3.0.CO;2-B

[31] M. Xu, D. Obodo, and V. K. Yadavalli, “The design, fabrication, and applications of flexible biosensing devices,” *Biosens Bioelectron*, vol. 124–125, pp. 96–114, Jan. 2019, doi: 10.1016/J.BIOS.2018.10.019.

[32] A. R. Cardoso et al., “Molecularly-imprinted chloramphenicol sensor with laser-induced graphene electrodes,” *Biosens Bioelectron*, vol. 124–125, pp. 167–175, Jan. 2019, doi: 10.1016/J.BIOS.2018.10.015.

[33] A. Baraket et al., “A Flexible Label-Free Biosensor Sensitive and Selective to TNF-α: Application for Chronic Heart Failure,” *Sensors & Transducers*, vol. 27, pp. 15–21, 2014, Accessed: Sep. 15, 2022. [Online]. Available: http://www.sensorsportal.com

[34] R. Nagarkar and J. Patel, “Polyvinyl Alcohol: A Comprehensive Study,” *Acta Scientific Pharmaceutical Sciences (ISSN: 2581-5423)*, vol.3, pp. 34 – 44, Apr. 2019.

[35] C. Horwood, “Ionic liquids as electrolytes for electrochemistry,” *Ionic Liquids in Analytical Chemistry*, pp. 329–342, Jan. 2022, doi: 10.1016/B978-0-12-823334-4.00012-6.

[36] M. Vafaiee, M. Vossoughi, R. Mohammadpour, and P. Sasanpour, “Gold-Plated Electrode with High Scratch Strength for Electrophysiological Recordings,” *Sci Rep*, vol. 9, no. 1, Dec. 2019, doi: 10.1038/S41598-019-39138-W.

[37] K. H. Goh, A. S. M. A. Haseeb, and Y. H. Wong, “Samarium Oxide and Samarium Oxynitride Thin Film as Alternative Gate Oxide on Silicon Substrate,” in *Reference Module in Materials Science and Materials Engineering*, Elsevier, 2017. doi: 10.1016/b978-0-12-803581-8.04073-x.

[38] Y. H. Wong and K. Y. Cheong, “ZrO 2 thin films on Si substrate,” *Journal of Materials Science: Materials in Electronics*, vol. 21, no. 10, pp. 980–993, Oct. 2010, doi: 10.1007/s10854-010-0144-5.

[39] K.W. Vogt, P.A. Kohl, W.B. Carter, R.A. Bell, L.A. Bottomley, “Characterization of thin titanium oxide adhesion layers on gold resistivity, morphology, and composition”, *Surface Science*, Volume 301, no. 1–3, 1994, pp. 203-213, doi: 10.1016/0039-6028(94)91300-5

[40] D. Titus, E. James Jebaseelan Samuel, and S. M. Roopan, “Nanoparticle characterization techniques,” *Green Synthesis, Characterization and Applications of Nanoparticles*, pp. 303–319, Jan. 2019, doi: 10.1016/B978-0-08-102579-6.00012-5.

[41] J. Yin, H. Hui, B. Fan, J. Bian, J. Du, and H. Yang, “Preparation and Properties of Polyimide Composite Membrane with High Transmittance and Surface Hydropho bicity for Lightweight Optical System,” *Membranes (Basel)*, vol. 12, no. 6, Jun. 2022, doi: 10.3390/membranes12060592.

[42] N. Raval, R. Maheshwari, D. Kalyane, S. R. Youngren-Ortiz, M. B. Chougule, and R. K. Tekade, “Importance of Physicochemical Characterization of Nanoparticles in Pharmaceutical Product Development,” *Basic Fundamentals of Drug Delivery*, pp. 369–400, Jan. 2019, doi: 10.1016/B978-0-12-817909-3.00010-8.

[43] J. Agostinho Gregório Dos Santos, “Ultrathin electronic tattoos (e-tattoo) for on-skin sensing,” Master thesis, Department of Materials Science, NOVA School of Science and Technology, Monte da Caparica, 2022.

[44] I. H. Hamzah, A. A. Manaf, and O. Sidek, “A Study on Characteristic and Reliability of Fabricated Microfluidic Three Electrodes Sensor Based on Randle-Sevcik Equation.” *2010 IEEE Asia Pacific Conference on Circuits and Systems*, 2010, pp. 816-819, doi: 10.1109/APCCAS.2010.5774816

[45] A. P. M. Tavares, L. A. A. N. A. Truta, F. T. C. Moreira, G. Minas, and M. G. F. Sales, “Photovoltaics, plasmonics, plastic antibodies and electrochromism combined for a novel generation of self-powered and self-signalled electrochemical biomimetic sensors,” *Biosens Bioelectron*, vol. 137, pp. 72–81, Jul. 2019, doi: 10.1016/j.bios.2019.04.055.

[46] R. S. Gomes, F. T. C. Moreira, R. Fernandes, and M. F. Goreti Sales, “Sensing CA 15-3 in point-of-care by electropolymerizing O-phenylenediamine (oPDA) on Au-screen printed electrodes,” *PLoS One*, vol. 13, no. 5, May 2018, doi: 10.1371/journal.pone.0196656.

[47] S. A. Gharaibeh, E. N. el Sawy, H. Molero, and V. I. Birss, “Electrochemical and Mass Change Study of the Growth of Poly-(o-Phenylenediamine) Films on Au Substrates,” *J Electrochem Soc*, vol. 160, no. 6, pp. H344–H354, Apr. 2013, doi: 10.1149/2.098306JES/XML.

[48] R. A. Lorenzo, A. M. Carro, C. Alvarez-Lorenzo, and A. Concheiro, “To Remove or Not to Remove? The Challenge of Extracting the Template to Make the Cavities Available in Molecularly Imprinted Polymers (MIPs),” *Int J Mol Sci*, vol. 12, no. 7, p. 4327, Jul. 2011, doi: 10.3390/IJMS12074327.

[49] “SIB Swiss Institute of Bioinformatics | Expasy.” https://www.expasy.org/ (accessed Dec. 21, 2022).

[50] “IL6 (human).” https://www.phosphosite.org/proteinAction?id=18622&showAllSites=true (accessed Dec. 21, 2022).

[51] “Pyrrole-3-carboxylic acid | 336100-46-0.” https://www.chemicalbook.com/ChemicalProductProperty_EN_CB6489171.htm (accessed Dec. 21, 2022).

[52] *CRC Handbook of Chemistry and Physics, 93rd Edition* - Google Livros, 93rd ed. Accessed: Sep. 25, 2022. [Online].

[53] O. J. Guy and K.-A. D. Walker, "Chapter 4 - Graphene Functionalization for Biosensor Applications," Elsevier, 2016, pp. 85-141, doi: 10.1016/B978-0-12-802993-0/00004-6.

[54] S. M. Sayyah, A. B. Khaliel, A. A. Aboud, and S. M. Mohamed, "Chemical polymerization kinetics of poly-O-phenylenediamine and characterization of the obtained polymer in aqueous hydrochloric acid solution using K2Cr2O7 as oxidizing agent," *Int J Polym Sci*, vol. 2014, Jun. 2014, doi: 10.1155/2014/520910.

[55] E. B. Aydın, "Highly sensitive impedimetric immunosensor for determination of interleukin 6 as a cancer biomarker by using conjugated polymer containing epoxy side groups modified disposable ITO electrode," *Talanta*, vol.215, Aug.2020, doi: 10.1016/j.talanta.2020.120909.

[56] E. B. Aydın, M. Aydın, and M. K. Sezgintürk, "A novel electrochemical immunosensor based on acetylene black/ epoxy-substituted-polypyrrole polymer composite for the highly sensitive and selective detection of interleukin 6," *Talanta*, vol. 222, p. 121596, 2021, doi: 10.1016/j.talanta.2020.121596.

[57] R. D. Munje, S. Muthukumar, B. Jagannath, and S. Prasad, "A new paradigm in sweat based wearable diagnostics biosensors using Room Temperature Ionic Liquids (RTILs)" *Sci Rep*, vol.7, May 2017, https://doi.org/10.1038/s41598-017-02133-0 doi: 10.1038/s41598-017-02133-0.

[58] M. Omidi et al., "Characterization of biomaterials," in *Biomaterials for Oral and Dental Tissue Engineering*, Elsevier Inc., 2017, pp. 97–115. doi: 10.1016/B978-0-08-100961-1.00007-4.

[59] P. Baran et al., "The balance of interleukin (IL)-6, IL-6·soluble IL-6 receptor (sIL-6R), and IL-6·sIL-6R·sgp130 complexes allows simultaneous classic and trans-signaling," *J Biol Chem*, vol. 293, no. 18, p. 6762, May 2018, doi: 10.1074/JBC.RA117.001163.

[60] J. J. Guirao, C. M. Cabrera, N. Jiménez, L. Rincón, and J. M. Urra, "High serum IL-6 values increase the risk of mortality and the severity of pneumonia in patients diagnosed with COVID-19," *Mol Immunol*, vol. 128, p. 64, Dec. 2020, doi: 10.1016/J.MOLIMM.2020.10.006.

[61] L. Y. C. Chen, R. L. Hoiland, S. Stukas, C. L. Wellington, and M. S. Sekhon, "Confronting the controversy: interleukin-6 and the COVID-19 cytokine storm syndrome," *European Respiratory Journal*, vol. 56, no. 4, Oct. 2020, doi: 10.1183/13993003.03006-2020.

[62] B. Byl', J. Devière, F. Saint-Hubert, F. Zech4, B. Gulbis', and J.-P. Thys, "Evaluation of tumor necrosis factor-a, interleukin-6 and C-reactive protein plasma levels as predictors of bacteremia in patients presenting signs of sepsis without shock," *Microbiol Infect.*, pp. 306-316, Jun. 1997, doi: 10.1111/j.1469-0691.1997.tb00618.x.

A
AN APPENDIX

A.1. Reagents

Regarding the membrane fabrication, both the adhesion promoter (VM652) and the polyimide (2611) were purchased from HD MicroSystems, and the poly (vinyl alcohol) (PVA, 8,8% hydrolysed, average M.W. 20000-30000) was obtained from Acros Organics. Potassium hexacyanoferrate II trihydrate ($K_4[Fe(CN)_6].3H_2O$) and potassium hexacyanoferrate III ($K_3[Fe(CN)_6]$) were obtained from Riedel-de-Haen. Citric acid ($C_6H_8O_7$) and sulphuric acid (H_2SO_4) were purchased from Sigma Aldrich. Potassium chloride (KCl) was purchased from Normapur and the isopropyl alcohol (IPA) was purchased from Honeywell. Dipotassium hydrogen phosphate (K_2HPO_4) was obtained from Fisher Chemical, potassium di-hydrogenophosphate (KH_2PO_4) was purchased from Panreac, sodium phosphate dibasic dihydrate, 99.5%, ($Na_2HPO_4.2H_2O$) was obtained from Carlos Erba and sodium hydroxide (NaOH) was purchased from EKA. As for the monomers, o-phenylenediamine (o-PDA, $C_6H_8N_2$) was obtained from Amresco, pyrrole, 98% (Py, C_4H_5N) and pyrrole-3-carboxylic acid (Py-COOH, $C_5H_5NO_2$) were purchased from Alfa Aesar; and 3,4-ethylenedioxythiophene, 98% (EDOT, $C_6H_6O_2S$) was obtained from TCI. The target protein interleukin 6, IL-6, was purchased from Abcam.

A.2. FTIR analysis

The measurements were performed in the Attenuated Total Reflectance (ATR) mode, using a Thermo Scientific Smart iTR Nicolet iS10, coupled with sampling accessory of germanium contact crystal, also from Nicolet. Infrared spectra were collected after background correction, with a number of scans set to 90 and the resolution was fixed at 16. FTIR data analysis was performed with OMNIC software.

A.3. XRD caracterizations

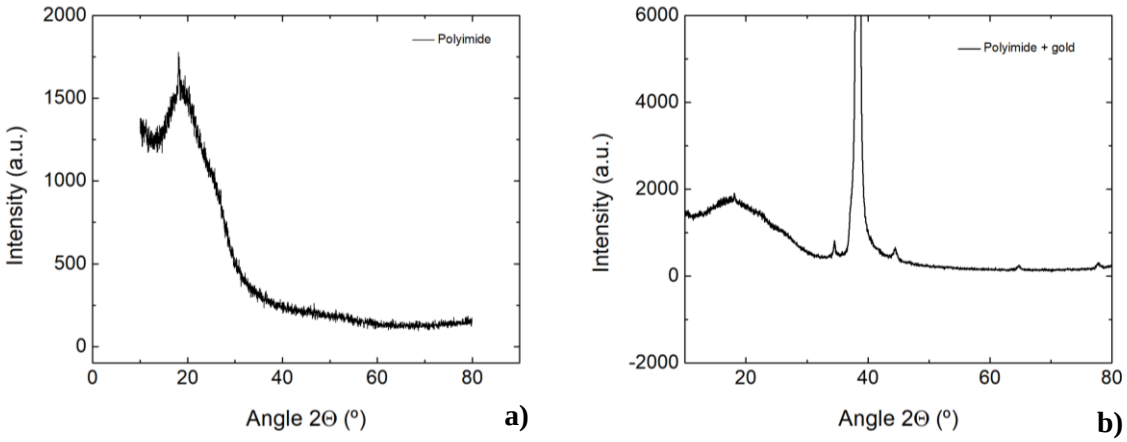

Figure A.3.1 - Membrane XRD analysis of a) polyimide membrane and b) polyimide membrane and gold layer

(2022) CAROLINA LOURENÇO

Development of a skin-like sensor for monitoring an inflammatory biomarker for wound care application

NOVA SCHOOL OF SCIENCE & TECHNOLOGY